A geometrically nonlinear three dimensional cohesive crack method for reinforced concrete structures

Timon Rabczuk [a] Goangseup Zi [b,*] Stéphane Bordas [c]
Hung Nguyen-Xuan [d]

[a] *Senior Lecturer, Department of Mechanical Engineering, University of Canterbury, Christchurch, New Zealand; Tel: +64-3-364-8836; Timon.Rabczuk@canterbury.ac.nz*

[b] *Assistant professor, Department of Civil, Environmental & Architectural Engineering, Korea University, 5 Ga 1, An-Am Dong, Sung-Buk Gu, Seoul, 136-701, Korea; Tel.: +82-2-3290-3324; g-zi@korea.ac.kr*

[c] *Lecturer (assistant professor), Civil Engineering Department, University of Glasgow, Rankine building, G12 8LT, Glasgow, UK; Tel: +44(0)141 330 4075; bordas@civil.gla.ac.uk*

[d] *Singapore-MIT Alliance (SMA), E4-04-10, 4 Engineering Drive 3, Singapore, 117576, National University of Singapore, 10 Kent Ridge Crescent 119260, Singapore; Tel.: +65 98604962; smanxh@nus.edu.sg*

Abstract

A three dimensional meshfree method for modeling arbitrary crack initiation and crack growth in reinforced concrete structure is presented. This meshfree method is based on a partition of unity concept and formulated for geometrically nonlinear problems. The crack kinematics are obtained by enriching the solution space in order to capture the correct crack kinematics. A cohesive zone model is used after crack initiation. The reinforcement modeled by truss or beam elements is connected by a bond model to the concrete. We applied the method to model the fracture of several reinforced concrete structures and compared the results to experimental data.

Key words: Prestressed concrete; Reinforced concrete; Cohesive zone modelling; Crack growth; Brittle fracture

Nomenclature

E Young's modulus of concrete

G_f fracture energy of concrete

H^+, H^- and ψ^+, ψ^- values of enrichment function on the plus and minus sides of a discontinuity

J Jacobian

$\Delta\mathbf{f}$ increment of force

$\Delta\boldsymbol{t}^c$ increment of the traction on crack surface

ΔT temperature change

α_t thermal expansion coefficient of prestressing tendon

$\mathbf{I}$ unit matrix

$\mathbf{R}$ rotation matrix

$[\![\mathbf{\Phi}]\!]$ matrix of the jump of the shape function

$\boldsymbol{S}$ second Piola-Kirchhoff stress

$\boldsymbol{\mathcal{B}}_0$ derivative of a shape function with respect to the initial reference coordinates

$\boldsymbol{t}^d$ interface traction on the deformable interface between concrete and reinforcement

ν Poisson's ratio of concrete

f_c compressive strength of concrete

k number of iteration

$\mathbf{B}$ B matrix

$\mathbf{C}^{\mathrm{ref},S}$, $\mathbf{C}^{\mathrm{con},S}$ modulus matrices of the second Piola-Kirchhoff stresses of reinforcement and concrete

$\mathbf{K}$ stiffness matrix

$\mathbf{T}^c$ modulus matrix of cohesive traction

$\mathbf{T}^d$ modulus matrix of interface traction

$\mathbf{\Phi}$ shape function matrix

$\mathbf{q}$ generalized nodal parameters

$\boldsymbol{X}$ coordinates in the initial configuration

* Corresponding author
Email address: g-zi@korea.ac.kr (Goangseup Zi).

$\bar{\boldsymbol{u}}$ prescribed displacements in the initial configuration

$\bar{\boldsymbol{t}}_0$ prescribed tractions in the initial configuration

$\boldsymbol{g}$ gap between reinforcement and concrete

$\boldsymbol{n}$ normal vector

$\boldsymbol{w}$ crack opening displacement

$\boldsymbol{x}$ position of a particle placed at $\boldsymbol{X}$ in the initial configuration

$f^{(n)}$ signed distance function with respect to crack (n)

h_I support size of shape function ϕ_I

n_c number of cracks that completely cross the domain of influence of a particle

n_t number of cracks that partially cross the domain of influence of a particle

$r^{(m)}(\boldsymbol{X})$ minimum distance of point $\boldsymbol{X}$ to the mth crack crack front

$\bar{\boldsymbol{b}}$ body force

$\mathbf{f}$ discretized force

$\mathbf{g}$ discretized gap between the reinforcement and the concrete

$\mathbf{r}$ residual of the discretized equilibrium equation

$\boldsymbol{a}_I$,$\boldsymbol{b}_I$ additional degrees of freedom for the enrichment functions for particle I

$\boldsymbol{t}_0^c$ cohesive traction across a crack in the initial configuration

$\boldsymbol{u}$ displacement vector or the trial function

H,ψ enrichment functions

H_I,ψ_I enrichment functions shifted with respect to particle I

$W(\boldsymbol{X}-\boldsymbol{X}_I, h_I)$ weight function of particle I

$\mathcal{R}$ set of all the nodes for reinforcement

$\mathcal{S}$ set of all particles

$\mathcal{S}_c$ subset of the particles whose domains of influence are completely cut by crack

$\mathcal{S}_t$ subset of the particles whose domains of influence are partially cut by crack

$\mathcal{V}$ space of the displacement or the trial function

$\mathcal{V}_0$ space of the test function

$\boldsymbol{F}$ deformation gradient tensor

$\boldsymbol{P}$ nominal stress tensor

$\boldsymbol{X}_{\text{tip}}^{(m)}$ mth crack crack front

δW virtual work

$\delta \dot{W}$ rate of the virtual work

$\delta \boldsymbol{u}$ test function

$\boldsymbol{\lambda}$ Lagrange multiplier

$\boldsymbol{\xi}$ local coordinates

ϕ shape function

$\theta^{(m)}(\boldsymbol{X})$ angle between the tangent to crack surface and segment $\boldsymbol{X} - \boldsymbol{X}_{\text{tip}}^{(m)}$

Γ boundary of domain Ω

Ω domain of body

$\boldsymbol{\Lambda}_I$ Lagrange multiplier parameter for particle I

∇ gradient operator

$_{\text{a}}$ subscript representing the degrees of freedom for the H enrichment

$_{\text{b}}$ subscript representing the degrees of freedom for the branch enrichment

^{c} superscript representing crack

$_{\text{coh}}$ subscript representing an cohesive mechanism

$^{\text{con}}$ superscript representing concrete

^{d} superscript representing the deformable interface between concrete and reinforcement

$_{e}$ subscript representing the enrichment or the discontinuity

$_{\text{ext}}$ subscript representing an external mechanism

$_{g}$ subscript representing the gap between concrete and reinforcement

$_{\text{geo}}$ subscript representing geometric effect

^{h} superscript representing an approximation

$_{\text{int}}$ subscript representing an internal mechanism

$_{\text{mat}}$ subscript representing the contribution of material

$^{\text{ref}}$ superscript representing reinforcement

$_{st}$ subscript representing the standard element free Galerkin method

$_{\text{u}}$ subscript representing the degrees of freedom for the continuous displacement

$_0$	subscript representing the initial reference configuration
$_\lambda$	subscript representing Lagrange multiplier
$_\Lambda$	subscript representing the degrees of freedom for a Lagrange multiplier
$^{(m)}$	index indicating a crack front (or tip)
$^{(n)}$	index indicating a crack
$^+, ^-$	signs for the crack surfaces
$_*$	subscript representing the virtual surface introduced between the deformed crack surfaces

1 Introduction

Reinforced concrete structures often undergo extensive cracking before failure. Tracking dense failure patterns by finite element methods is quite difficult. Therefore, particle methods are very attractive for this class of problems.

In early approaches, cracks in the concrete were modeled by strain softening in the stress-strain curve, see e.g. [1]. Such continuum models are mesh-dependent if no modifications are made to reflect mesh spacing since a finer discretization leads to a decrease in fracture energy. Other approaches are fictitious crack and smeared crack models, see e.g. [2–5]. In those models, a crack is assumed to be within an integration cell. Usually the strains are related to a *fictitious* crack width in the integration cell. In smeared crack models, we have to distinguish whether a single or several cracks should be modeled within a single integration cell. If larger structures such as shells are of interest, more than one crack can be initiated in an element. The advantage of fictitious or smeared crack models is that the cracks are initiated through the constitutive model in contrast to discrete crack models; the crack is not considered as a distinct discontinuity. Hence, these models are called the weak discontinuity approaches.

Discrete crack models are an alternative to fictitious crack models. These models are called strong discontinuity models because the formation of a crack is modeled by using a discontinuity introduced in the solution space. A possibility for introducing discrete cracks was studied by Xu and Needleman [14, 15] who separated elements at their boundaries. This approach has the disadvantage that the crack propagation depends on the geometry and the topology of the mesh. Remeshing and refinement could overcome this drawback but these approaches are computationally expensive. The Cornell group of Ingraffea has developed remeshing to a high degree of robustness (see e.g. [16, 17]), but three dimensional problems with multiple cracks appear to be very challenging by using these methods. Recently, a new kind of discrete crack method called the extended finite element method (XFEM) was developed based on

the local partition of unity by Belytschko and his collaborators [18–21] where the crack can propagate arbitrarily in an element without remeshing. Either the elements or the nodes are enriched with additional degrees of freedom.

Meshfree methods are a good alternative to finite elements for crack problems. In addition to the advantage of being more flexible because of the lack of a mesh, they have the nonlocal interpolation character [1] which provides higher smoothness and continuity. Modeling cracks with meshfree methods was first proposed by Belytschko et al. [22–25]. The crack was modeled by using a visibility criterion where the domain of influence was cut by a crack. The concept of local partition of unity and level sets were incorporated in a meshfree context for linear elastic cracks by Ventura [26] and for cohesive cracks by Rabczuk and Zi [27].

In this paper, we present a three-dimensional cohesive crack method for reinforced concrete structures. We model cracking in the concrete with an extended element-free Galerkin method (XEFG) that is coupled to finite elements for the reinforcement following the general formulation of geometrically nonlinear problems. The ill-posed IBVP is treated by means of cohesive surfaces in the post localization domain.

Another important issue when modeling reinforced concrete structures is the interaction between the concrete and the reinforcement. If a rigid connection between the concrete and the reinforcement is assumed, the experimental crack pattern usually cannot be well reproduced. In reality, the stresses in the reinforcement increase around the cracked concrete and unloading occurs in the vicinity of the crack which causes cracks at a certain distance from each other. Without a bond model, this effect cannot be captured and cracks occur over the entire length of the reinforcement in certain applications.

According to Cox and Herrmann [28, 29], bond models can be developed at three different scales, the *ribscale*, where the geometry of the surface structure of the bar is modeled explicitly; and the *barscale* and the *memberscale*, where

[1] the method is not non-local in the constitutive sense as described above

the reinforcement is discretized via a discrete, embedded or smeared model. In the member scale model, the reinforcement is treated as a one-dimensional element. Bond laws have been limited to single-stress models and are not well suited to reproduce the complicated bond behavior in certain cases. For our applications, we selected a model at the *barscale*. We used a bond model described in detail in [30] which can also capture both modes *I* and *II* bond failure mechanisms.

The paper is arranged as follows: First, we give the governing equations. The particle-finite element method and the cracking approach are briefly reviewed. Then, we describe the coupling scheme for deformable interfaces. Finally, we describe our testing of the approach for various problems.

2 Governing equations

The governing equation is the equation of equilibrium given by

$$\nabla_0 \cdot \boldsymbol{P} - \bar{\boldsymbol{b}} = \boldsymbol{0} \quad \forall \quad \boldsymbol{X} \in \Omega_0 \setminus \Gamma_0^c \tag{1}$$

where $\boldsymbol{P}$ is the nominal stress tensor (see [31] for details), $\bar{\boldsymbol{b}}$ is the body force, $\boldsymbol{X}$ are the material coordinates, ∇_0 is the gradient operator with respect to the initial reference coordinates, Γ_0^c is the crack surface and Ω_0 is the domain of the body. The boundary conditions are

$$\boldsymbol{u}(\boldsymbol{X},t) = \bar{\boldsymbol{u}}(\boldsymbol{X},t) \quad \text{on} \quad \Gamma_0^u \tag{2}$$

$$\boldsymbol{n}_0 \cdot \boldsymbol{P}(\boldsymbol{X},t) = \bar{\boldsymbol{t}}_0(\boldsymbol{X},t) \quad \text{on} \quad \Gamma_0^t \tag{3}$$

$$\boldsymbol{n}_0^c \cdot \boldsymbol{P}^- = \boldsymbol{n}_0^c \cdot \boldsymbol{P}^+ = \boldsymbol{t}_0^c \text{ on } \Gamma_0^c \tag{4}$$

where $\bar{\boldsymbol{u}}$ and $\bar{\boldsymbol{t}}_0$ are the prescribed displacements and tractions, respectively, $\boldsymbol{t}_0^c$ are the cohesive traction across the crack, $\boldsymbol{n}_0^c$ is the crack normal in the initial configuration and $\Gamma_0^u \bigcup \Gamma_0^t = \Gamma_0$, $\Gamma_0^u \bigcap \Gamma_0^t = \varnothing$.

The weak form of the equilibrium equation is given by

$$\delta W = \delta W_{\text{ext}} + \delta W_{\text{coh}} - \delta W_{\text{int}} = 0 \tag{5}$$

with

$$\begin{aligned}
\delta W_{\text{int}} &= \int_{\Omega_0 \setminus \Gamma_0^c} \delta \boldsymbol{F}^T : \boldsymbol{P} \, \mathrm{d}\Omega_0 \\
&= \int_{\Omega_0 \setminus \Gamma_0^c} \delta \boldsymbol{F}^T : \left(\boldsymbol{S} \cdot \boldsymbol{F}^T \right) \, \mathrm{d}\Omega_0 \qquad (6) \\
\delta W_{\text{ext}} &= \int_{\Omega_0} \delta \boldsymbol{u} \cdot \bar{\boldsymbol{b}} \, \mathrm{d}\Omega_0 - \int_{\Gamma_0^t} \delta \boldsymbol{u} \cdot \bar{\boldsymbol{t}}_0 \, \mathrm{d}\Gamma_0 \qquad (7) \\
\delta W_{\text{coh}} &= \int_{\Gamma_0^{c+}} \delta \boldsymbol{u}^+ \cdot \boldsymbol{t}_0^{c+} \, \mathrm{d}\Gamma_0 + \int_{\Gamma_0^{c-}} \delta \boldsymbol{u}^- \cdot \boldsymbol{t}_0^{c-} \, \mathrm{d}\Gamma_0 \\
&= - \int_{\Gamma_0^c} \delta [\![\boldsymbol{u}]\!] \cdot \boldsymbol{t}_0^c \, \mathrm{d}\Gamma_0 \qquad (8)
\end{aligned}$$

$\boldsymbol{F} = \boldsymbol{x} \otimes \nabla_0$ is the deformation gradient tensor and $\boldsymbol{u}$ and $\delta \boldsymbol{u}$ are the trial and test functions which should lie in the following spaces

$$\begin{aligned}
\mathcal{V} &= \left\{ \boldsymbol{u} | \boldsymbol{u} \in \mathcal{H}^1, \ \boldsymbol{u} \text{ discontinuous on } \Gamma_0^c, \ \boldsymbol{u} = \bar{\boldsymbol{u}} \text{ on } \Gamma_0^u \right\} \\
\mathcal{V}_0 &= \left\{ \delta \boldsymbol{u} | \delta \boldsymbol{u} \in \mathcal{H}^1, \ \delta \boldsymbol{u} \text{ discontinuous on } \Gamma_0^c, \ \delta \boldsymbol{u} = 0 \text{ on } \Gamma_0^u \right\} \qquad (9)
\end{aligned}$$

In Eq. (8), the relation of $\boldsymbol{t}_0^c = \boldsymbol{t}_0^{c-} = -\boldsymbol{t}_0^{c+}$ is used.

The rates of the virtual works in Eqs. (6) to (8) are given by

$$\begin{aligned}
\delta \dot{W}_{\text{int}} &= \int_{\Omega_0 \setminus \Gamma_0^c} \delta \boldsymbol{F}^T : \left(\dot{\boldsymbol{S}} \cdot \boldsymbol{F}^T + \boldsymbol{S} \cdot \dot{\boldsymbol{F}}^T \right) \, \mathrm{d}\Omega_0 \\
&= \int_{\Omega_0 \setminus \Gamma_0^c} \delta \boldsymbol{F}^T : \left(\dot{\boldsymbol{S}} \cdot \boldsymbol{F}^T \right) \, \mathrm{d}\Omega_0 + \int_{\Omega_0 \setminus \Gamma_0^c} \delta \boldsymbol{F}^T : \left(\boldsymbol{S} \cdot \dot{\boldsymbol{F}}^T \right) \, \mathrm{d}\Omega_0 \qquad (10) \\
\delta \dot{W}_{\text{ext}} &= \int_{\Omega_0} \delta \boldsymbol{u} \cdot \dot{\bar{\boldsymbol{b}}} \, \mathrm{d}\Omega_0 - \int_{\Gamma_0^t} \delta \boldsymbol{u} \cdot \dot{\bar{\boldsymbol{t}}}_0 \, \mathrm{d}\Gamma_0 \qquad (11) \\
\delta \dot{W}_{\text{coh}} &= - \int_{\Gamma_0^c} \delta [\![\boldsymbol{u}]\!] \cdot \left[\boldsymbol{n}_0 \cdot \left(\dot{\boldsymbol{S}} \cdot \boldsymbol{F}^T + \boldsymbol{S} \cdot \dot{\boldsymbol{F}}^T \right) \right] \, \mathrm{d}\Gamma_0 \qquad (12)
\end{aligned}$$

Note that because of the discontinuity Γ_0^c, the crack normal $\boldsymbol{n}$ in the deformed configuration corresponding to the normal $\boldsymbol{n}_0$ in the initial configuration is not unique.

3 The element free galerkin method (EFG)

The standard EFG-approximation [2] is used to model the concrete. The displacement approximation in EFG is given by

$$\boldsymbol{u}^h_{st}(\boldsymbol{X},t) = \sum_{I\in\mathcal{S}} \phi_I(\boldsymbol{X})\ \boldsymbol{u}_I(t) \tag{13}$$

where the subscript st denotes the standard EFG approximation, $\phi_I(\boldsymbol{X})$ are the shape functions, $\mathcal{S}$ is the set of all particles, $\boldsymbol{u}_I$ is the displacement parameter of a particle positioned at $\boldsymbol{X}_I$, $W(\boldsymbol{X}-\boldsymbol{X}_I, h_I)$ is the weight function and h_I is the support size of shape function ϕ_I. Using the moving least square method, we obtain the shape functions

$$\phi_I = \boldsymbol{p}^T(\boldsymbol{X})\cdot\ \boldsymbol{A}(\boldsymbol{X})^{-1}\cdot\boldsymbol{D}(\boldsymbol{X}) \tag{14}$$

with the moment matrix

$$\boldsymbol{A}(\boldsymbol{X}) = \sum_{I\in S}\ \boldsymbol{p}_I(\boldsymbol{X})\ \boldsymbol{p}_I^T(\boldsymbol{X})\, W(\boldsymbol{X}-\boldsymbol{X}_I, h_0) \tag{15}$$

$$\boldsymbol{D}(\boldsymbol{X}) = \sum_{I\in S}\ \boldsymbol{p}_I(\boldsymbol{X})\, W(\boldsymbol{X}-\boldsymbol{X}_I, h_I) \tag{16}$$

4 A coupled particle-finite element approach for reinforced concrete

4.1 A Method for the rigid bond using Lagrange multipliers

The displacements of the two domains, i.e. the reinforcement and the concrete, are denoted by $\boldsymbol{u}^{\text{ref}}$ and $\boldsymbol{u}^{\text{con}}$, respectively. Since it is assumed that there is no fracture of the reinforcement, the displacement of the reinforcement can be approximated by the standard finite element method.

$$\boldsymbol{u}^{\text{ref},h}(\boldsymbol{X}) = \sum_{J\in\mathcal{R}} \phi^{\text{ref}}_J(\boldsymbol{X})\ \boldsymbol{u}^{\text{ref}}_J \tag{17}$$

[2] see [22, 23, 32, 33] for details

in which $\mathcal{R}$ is the set of all the nodes for the reinforcement. Because of the cracks in the concrete, the displacement space of the standard EFG is enriched by the discontinuous displacement $\boldsymbol{u}_e$ [27, 34, 35]. The displacement approximation for the concrete is given by

$$\begin{aligned}\boldsymbol{u}^{\mathrm{con},h}(\boldsymbol{X}) = &\sum_{I\in\mathcal{S}} \phi_I^{\mathrm{con}}(\boldsymbol{X},t)\ \boldsymbol{u}_I^{\mathrm{con}} + \sum_{n=1}^{n_c}\sum_{I\in\mathcal{S}_c} \phi_I^{\mathrm{con}}(\boldsymbol{X})\ H_I^{(n)}(\boldsymbol{X})\ \boldsymbol{a}_I^{(n)} \\ &+ \sum_{m=1}^{m_t}\sum_{I\in\mathcal{S}_t} \phi_I^{\mathrm{con}}(\boldsymbol{X})\psi_I^{(m)}(\boldsymbol{X})\ \boldsymbol{b}_I^{(m)} \end{aligned} \tag{18}$$

where $\mathcal{S}_c$ is the subset of the particles whose domains of influence are completely cut by the crack, $\mathcal{S}_t$ is the subset of the particles whose domains of influence are partially cut by the crack, n_c and m_t are the number of cracks that completely or partially cross the domain of influence of a corresponding particle, H and ψ are the enrichment functions, $\boldsymbol{a}$ and $\boldsymbol{b}$ are additional unknowns introduced to represent the discontinuity across the crack faces and the asymptotic stress state near the crack tip, respectively. The last two terms of Eq. (18) are the enrichment.

The enrichment function H_I is given by

$$H_I^{(n)}(\boldsymbol{X}) = \mathrm{sign}\left[f^{(n)}(\boldsymbol{X}) \right] - \mathrm{sign}\left[f^{(n)}(\boldsymbol{X}_I) \right] \tag{19}$$

in which $f^{(n)}$ is the signed distance function with respect to crack (n) defined as

$$f^{(n)}(\boldsymbol{X}) = \mathrm{sign}\left[\boldsymbol{n}_0 \cdot (\boldsymbol{X} - \boldsymbol{X}^{(n)}) \right] \min_{\boldsymbol{X}^{(n)}\in\Gamma_0^{c,(n)}} \left\| \boldsymbol{X} - \boldsymbol{X}^{(n)} \right\| \tag{20}$$

where $\Gamma_0^{c,(n)}$ is the nth crack. If the signed distance function should be calculated for a point $\boldsymbol{X}$ beyond the crack tip of $\Gamma_0^{c,(n)}$, $\boldsymbol{X}^{(n)}$ is chosen from the tangent at the closest tip. The enrichment function ψ_I is the branch enrichment given by

$$\psi_I^{(m)} = {r^{(m)}}^k(\boldsymbol{X}) \sin\frac{\theta^{(m)}(\boldsymbol{X})}{2} - {r^{(m)}}^k(\boldsymbol{X}_I) \sin\frac{\theta^{(m)}(\boldsymbol{X}_I)}{2} \quad \text{for } k \geq 1 \tag{21}$$

where $r^{(m)}(\boldsymbol{X})$ is the minimum distance of $\boldsymbol{X}$ to the mth crack crack front $\boldsymbol{X}_{\mathrm{tip}}^{(m)}$ and $\theta^{(m)}(\boldsymbol{X}) = \sin^{-1}\left[f^{(m)}(\boldsymbol{X})/r^{(m)}(\boldsymbol{X}) \right]$ is the angle between the tangent to the crack surface and the segment $\boldsymbol{X} - \boldsymbol{X}_{\mathrm{tip}}^{(m)}$.

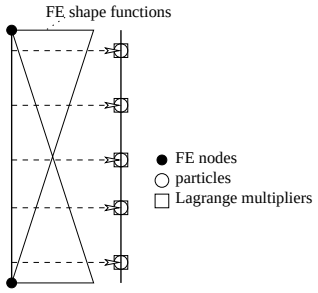

Fig. 1. Coupling using the Lagrange multipliers

The crack opening displacement $\boldsymbol{w}$ is measured as

$$\boldsymbol{w} = \sum_{n=1}^{n_c} \sum_{I \in \mathcal{S}_c} \left[\!\left[\phi_I H_I^{(n)} \right]\!\right] \boldsymbol{a}_I^{(n)} + \sum_{m=1}^{m_t} \sum_{I \in \mathcal{S}_t} \left[\!\left[\phi_I \psi_I^{(m)} \right]\!\right] \boldsymbol{b}_I^{(m)} \tag{22}$$

Let us assume a rigid bond between the reinforcement and the concrete, i.e. between the finite element and particle domain. In order to ensure the displacement continuity between the reinforcement and the concrete, the variational principle in Eq. (5) is to be modified by introducing a Lagrange multiplier, i.e.

$$\delta W = \delta W_{\text{ext}} + \delta W_{\text{coh}} + \delta W_{\lambda} - \delta W_{\text{int}} \quad \text{with} \quad \delta W_{\lambda} = \delta \left(\boldsymbol{g} \cdot \boldsymbol{\lambda} \right) \tag{23}$$

where δW_{λ} is the virtual work by the Lagrange multiplier $\boldsymbol{\lambda}$ and $\boldsymbol{g}$ is the gap between the reinforcement and the concrete, respectively. The Lagrange multiplier can be considered as a traction along the interface. The gap and its approximation are given by

$$\boldsymbol{g} = \boldsymbol{u}^{\text{ref}} - \boldsymbol{u}^{\text{con}} \tag{24}$$

$$\begin{aligned} \boldsymbol{g}^h = & \sum_{I \in \mathcal{R}} \phi_I^{\text{ref}}(\boldsymbol{X})\ \boldsymbol{u}_I^{\text{ref}} - \sum_{I \in \mathcal{S}} \phi_I^{\text{con}}(\boldsymbol{X}, t)\ \boldsymbol{u}_I^{\text{con}} - \sum_{n=1}^{n_c} \sum_{I \in \mathcal{S}_c} \phi_I^{\text{con}}(\boldsymbol{X})\ H_I^{(n)}(\boldsymbol{X})\ \boldsymbol{a}_I^{(n)} \\ & - \sum_{m=1}^{m_t} \sum_{I \in \mathcal{S}_t} \phi_I^{\text{con}}(\boldsymbol{X}) \phi_I^{(m)}(\boldsymbol{X})\ \boldsymbol{b}_I^{(m)} \end{aligned} \tag{25}$$

We use the finite element shape functions to discretize the Lagrange multiplier $\boldsymbol{\lambda}$, i.e.

$$\boldsymbol{\lambda}^h(\boldsymbol{X}) = \sum_{I \in \mathcal{R}} \phi_I^{\lambda}(\boldsymbol{X})\ \boldsymbol{\Lambda}_I \tag{26}$$

where $\phi_I^{\lambda}(\boldsymbol{X})$ are the shape functions for the Lagrange multiplier. For the interpolation in Eq. (26), the position of the Lagrange multipliers in the local

element coordinate system has to be known. Since the global positions of the nodes are known, then the local position can simply be obtained from $\Phi_I^\lambda(\boldsymbol{\xi})\boldsymbol{X}_I$ with respect to the local coordinates $\boldsymbol{\xi}$, see Fig. 1.

It is trivial to show the derivation of the test functions from the trial functions in Eqs. (17,18) and (25,26). Substituting the test and trial functions into the weak form Eq. (23), we obtain this discretized equilibrium equation

$$\mathbf{r} = \begin{Bmatrix} \mathbf{r}_f \\ \mathbf{r}_g \end{Bmatrix} = \begin{Bmatrix} \mathbf{f}_{\text{ext}} + \mathbf{f}_{\text{coh}} + \mathbf{f}_\lambda - \mathbf{f}_{\text{int}} \\ \mathbf{g} \end{Bmatrix} = \mathbf{0} \tag{27}$$

The discretized forces are given by

$$\mathbf{f}_{\text{int}} = \int_{\Omega_0^{\text{ref}}} \left[\, \mathbf{B}_{0u}^{\text{ref}} \,\right]^T \left\{ \boldsymbol{S}^{\text{ref}} \right\} \mathrm{d}\Omega_0 + \int_{\Omega_0^{\text{con}} \setminus \Gamma_0^c} \left[\, \mathbf{B}_0^{\text{con}} \,\right]^T \left\{ \boldsymbol{S}^{\text{con}} \right\} \mathrm{d}\Omega_0 \tag{28}$$

$$\mathbf{f}_{\text{ext}} = \int_{\Omega_0^{\text{con}} \setminus \Gamma_0^c} \left[\, \boldsymbol{\Phi}^{\text{con}} \,\right]^T \bar{\boldsymbol{b}} \, \mathrm{d}\Omega_0 + \int_{\Gamma_0^t} \left[\, \boldsymbol{\Phi}^{\text{con}} \,\right]^T \bar{\boldsymbol{t}}_0 \, \mathrm{d}\Gamma_0 \tag{29}$$

$$\mathbf{f}_{\text{coh}} = -\int_{\Gamma_0^c} [\![\boldsymbol{\Phi}^{\text{con}}]\!]^T \boldsymbol{t}_0^c \, \mathrm{d}\Gamma_0 \tag{30}$$

$$\mathbf{f}_\lambda = \int_{\Gamma_0^\lambda} \left[\, \boldsymbol{\Phi}_u^{\text{ref}} \quad - \boldsymbol{\Phi}^{\text{con}} \,\right]^T \left[\, \boldsymbol{\Phi}_u^\lambda \,\right] \, \mathrm{d}\Gamma_0 \, \boldsymbol{\Lambda} \tag{31}$$

$$\begin{aligned} \mathbf{g} = & \int_{\Gamma_0^\lambda} \left[\, \boldsymbol{\Phi}_u^\lambda \,\right]^T \left[\, \boldsymbol{\Phi}_u^{\text{ref}} \,\right] \, \mathrm{d}\Gamma_0 \, \mathbf{u}^{\text{ref}} - \int_{\Gamma_0^\lambda} \left[\, \boldsymbol{\Phi}_u^\lambda \,\right]^T \left[\, \boldsymbol{\Phi}_u^{\text{con}} \,\right] \, \mathrm{d}\Gamma_0 \, \mathbf{u}^{\text{con}} \\ & - \int_{\Gamma_0^\lambda} \left[\, \boldsymbol{\Phi}_u^\lambda \,\right]^T \left[\, \boldsymbol{\Phi}_a^{\text{con}} \,\right] \, \mathrm{d}\Gamma_0 \, \mathbf{a}^{\text{con}} - \int_{\Gamma_0^\lambda} \left[\, \boldsymbol{\Phi}_u^\lambda \,\right]^T \left[\, \boldsymbol{\Phi}_b^{\text{con}} \,\right] \, \mathrm{d}\Gamma_0 \, \mathbf{b}^{\text{con}} \end{aligned} \tag{32}$$

in which Γ_0^λ is the interface between the reinforcement and the concrete, $\boldsymbol{S}$ is the second Piola-Kirchhoff stress, $\mathbf{B}_0^{\text{con}} = [\, \mathbf{B}_{0u}^{\text{con}} \;\; \mathbf{B}_{0a}^{\text{con}} \;\; \mathbf{B}_{0b}^{\text{con}} \,]$, $\boldsymbol{\Phi}^{\text{con}} = [\, \boldsymbol{\Phi}_u^{\text{con}} \;\; \boldsymbol{\Phi}_a^{\text{con}} \;\; \boldsymbol{\Phi}_b^{\text{con}} \,]$, $[\![\boldsymbol{\Phi}^{\text{con}}]\!] = \left[\!\!\left[\, \boldsymbol{\Phi}_a^{\text{con}} \;\; \boldsymbol{\Phi}_b^{\text{con}} \,\right]\!\!\right]$, $\mathbf{B}_{0\diamond}^\dagger = (B_{0\diamond})_{ikjI}^\dagger = \underset{i,k}{\text{sym}} \left(\frac{\partial \varphi_I^\diamond}{\partial X_i} F_{jk} \right)^\dagger$, $\varphi_I^\diamond$ represents a shape function with enrichment $\diamond$, e.g. $\varphi_I^a = \phi_I \, H_I$ and

$$\begin{aligned} & \left[\, \boldsymbol{\Phi}_u^{\text{ref}} \,\right] = \left[\, \boldsymbol{\Phi}^{\text{ref}} \,\right] = \left[\, \phi_I^{\text{ref}} \,\right] && \forall I \in \mathcal{R} \\ & \left[\, \boldsymbol{\Phi}_u^{\text{con}} \,\right] = \left[\, \phi_I^{\text{con}} \,\right] && \forall I \in \mathcal{S} \\ & \left[\, \boldsymbol{\Phi}_a^{\text{con}} \,\right] = \left[\, \phi_I^{\text{con}} H_I^{(n)} \,\right] && \forall I \in \mathcal{S}_c \;\text{ and }\; n = 1, 2, \ldots, n_c \\ & \left[\, \boldsymbol{\Phi}_b^{\text{con}} \,\right] = \left[\, \phi_I^{\text{con}} B_I^{(m)} \,\right] && \forall I \in \mathcal{S}_t \;\text{ and }\; m = 1, 2, \ldots, m_t \\ & \left[\!\!\left[\, \boldsymbol{\Phi}_a^{\text{con}} \,\right]\!\!\right] = \left[\, \phi_I^{\text{con}} [\![H_I^{(n)}]\!] \,\right] && \forall I \in \mathcal{S}_c \;\text{ and }\; n = 1, 2, \ldots, n_c \\ & \left[\!\!\left[\, \boldsymbol{\Phi}_b^{\text{con}} \,\right]\!\!\right] = \left[\, \phi_I^{\text{con}} [\![B_I^{(m)}]\!] \,\right] && \forall I \in \mathcal{S}_t \;\text{ and }\; m = 1, 2, \ldots, m_t \end{aligned} \tag{33}$$

The residual in Eq. (27) can be linearized to

$$\mathbf{r}^k(\mathbf{q}) + \left.\frac{\partial \mathbf{r}(\mathbf{q})}{\partial \mathbf{q}}\right|_k \Delta\mathbf{q}^{k+1} = \mathbf{0} \tag{34}$$

where k is the number of the iteration and $\mathbf{q} = [\,\mathbf{u}^{\mathrm{ref}} \quad \mathbf{u}^{\mathrm{con}} \quad \mathbf{a}^{\mathrm{con}} \quad \mathbf{b}^{\mathrm{con}} \quad \mathbf{\Lambda}\,]^T$ are the generalized nodal parameters. Assuming that the body forces and the external tractions do not depend on $\mathbf{q}$, we obtain

$$\frac{\partial \mathbf{r}(\mathbf{q})}{\partial \mathbf{q}} = \left\{ \begin{array}{l} \frac{\partial \mathbf{f}_{\mathrm{coh}}(\mathbf{q})}{\partial \mathbf{q}} + \frac{\partial \mathbf{f}_{\lambda}(\mathbf{q})}{\partial \mathbf{q}} - \frac{\partial \mathbf{f}_{\mathrm{int}}(\mathbf{q})}{\partial \mathbf{q}} \\ \frac{\partial \mathbf{g}(\mathbf{q})}{\partial \mathbf{q}} \end{array} \right\} \tag{35}$$

The linearized terms for Eq. (35) can be obtained from the rate of the virtual work given in Eqs. (10-12). The increment of the internal force $\Delta\mathbf{f}_{\mathrm{int}}$ is given by

$$\begin{aligned} \Delta\mathbf{f}_{\mathrm{int}} = & \int_{\Omega_0^{\mathrm{ref}}} \left[\, \mathbf{B}_{0u}^{\mathrm{ref}} \,\right]^T \mathbf{C}^{\mathrm{ref},S} \left[\, \mathbf{B}_{0u}^{\mathrm{ref}} \,\right] \mathrm{d}\Omega_0 \, \Delta\mathbf{u}^{\mathrm{ref}} \\ & + \int_{\Omega_0^{\mathrm{con}} \setminus \Gamma_0^c} [\, \mathbf{B}_0^{\mathrm{con}} \,]^T \mathbf{C}^{\mathrm{con},S} [\, \mathbf{B}_0^{\mathrm{con}} \,] \, \mathrm{d}\Omega_0 \, \Delta\mathbf{q}^{\mathrm{con}} \\ & + \mathbf{I} \int_{\Omega_0^{\mathrm{ref}}} \left[\, \boldsymbol{\mathcal{B}}_{0u}^{\mathrm{ref}} \,\right]^T \left\{ \boldsymbol{S}^{\mathrm{ref}} \right\} \left[\, \boldsymbol{\mathcal{B}}_{0u}^{\mathrm{ref}} \,\right] \mathrm{d}\Omega_0 \, \Delta\mathbf{u}^{\mathrm{ref}} \\ & + \mathbf{I} \int_{\Omega_0^{\mathrm{con}} \setminus \Gamma_0^c} [\, \boldsymbol{\mathcal{B}}_0^{\mathrm{con}} \,]^T \{ \boldsymbol{S}^{\mathrm{con}} \} [\, \boldsymbol{\mathcal{B}}_0^{\mathrm{con}} \,] \, \mathrm{d}\Omega_0 \, \Delta\mathbf{q}^{\mathrm{con}} \end{aligned} \tag{36}$$

in which $\mathbf{C}^{\mathrm{ref},S}$ and $\mathbf{C}^{\mathrm{con},S}$ are the modulus matrices of the second Piola-Kirchhoff stresses of the reinforcement and the concrete, $\mathbf{q}^{\mathrm{con}} = [\,\mathbf{u}^{\mathrm{con}} \;\; \mathbf{a}^{\mathrm{con}} \;\; \mathbf{b}^{\mathrm{con}}\,]^T$ are the nodal parameters for the concrete, $\boldsymbol{\mathcal{B}}_0 = \mathcal{B}_{jI} = \partial\varphi_I/\partial X_j$ and $\mathbf{I}$ is the unit matrix. The first two terms in Eq. (36) are because of the material nonlinearity and the second two terms the geometric nonlinearity.

The increment of the Lagrange multiplier $\Delta\mathbf{f}_{\lambda}$ is simply given by

$$\Delta\mathbf{f}_{\lambda} = \int_{\Gamma_0^{\lambda}} \left[\, \mathbf{\Phi}_u^{\mathrm{ref}} \quad -\mathbf{\Phi}^{\mathrm{con}} \,\right]^T \left[\, \mathbf{\Phi}_u^{\lambda} \,\right] \mathrm{d}\Gamma_0 \, \Delta\mathbf{\Lambda} \tag{37}$$

The linearization of the cohesive force is not straightforward because of the discontinuity. Once a crack forms, the material point splits into two. Therefore a normal $\boldsymbol{n}_0^c$ to the crack surface in the initial configuration becomes two

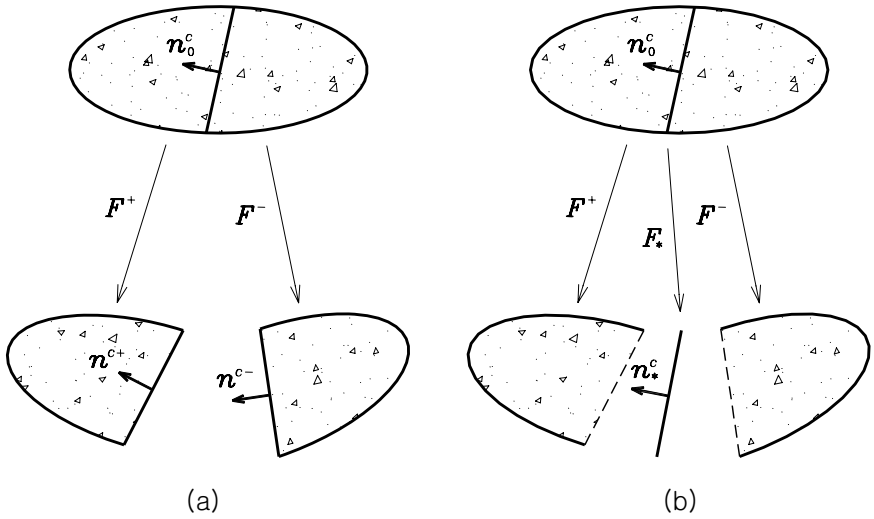

Fig. 2. (a) The deformation of a cracked body and (b) a new surface introduced between the crack surfaces and their deformation gradient tensor.

different crack normals $\boldsymbol{n}^{c+}$ and $\boldsymbol{n}^{c-}$ to the crack surface by deformation (Fig. 2). Nanson's formula for the transformation of a normal in a continuous body cannot be used because of that reason. To overcome this problem, Wells et al. [36] introduced a virtual surface Γ_*^c between the deformed crack surface Γ^{c+} and Γ^{c-}. The initial crack normal $\boldsymbol{n}_0$ was transformed to $\boldsymbol{n}_*$ on this new surface Γ_*^c by Nanson's formula; see Fig. 2. For this, Nanson's formula was modified:

$$\boldsymbol{n}_* \, \mathrm{d}\Gamma_* = J \boldsymbol{n}_0 \cdot \boldsymbol{F}^{*-1} \, \mathrm{d}\Gamma_0 \tag{38}$$

where $J = \det \boldsymbol{F}_*$ and $\boldsymbol{F}_*$ is the deformation gradient of the newly defined surface Γ_*^c between the deformed crack surfaces Γ^{c+} and Γ^{c-}. In our problem, $\boldsymbol{F}_*$ is simply defined as

$$\boldsymbol{F}_* = \frac{1}{2} \left(\boldsymbol{F}^+ + \boldsymbol{F}^- \right) \tag{39}$$

Using the above simplification, we obtain the increment of the cohesive force:

$$\begin{aligned} \Delta \boldsymbol{f}_{\mathrm{coh}} &= - \left(\int_{\Gamma_*^c} [\![\boldsymbol{\Phi}^{\mathrm{con}}]\!]^T \, \Delta \boldsymbol{t}^c \mathrm{d}\Gamma_* + \int_{\Gamma_*^c} [\![\boldsymbol{\Phi}^{\mathrm{con}}]\!]^T \, \boldsymbol{t}^c \, [\, \mathbf{B}_*^{\mathrm{con}} \,] \, \mathrm{d}\Gamma_* \, \Delta \mathbf{q}^{\mathrm{con}} \right) \\ &= - \int_{\Gamma_*^c} [\![\boldsymbol{\Phi}^{\mathrm{con}}]\!]^T \, \mathbf{R} \, \mathbf{T}^c \, \mathbf{R}^T [\![\boldsymbol{\Phi}^{\mathrm{con}}]\!] \, \mathrm{d}\Gamma_* \, [\, \Delta \mathbf{a}^{\mathrm{con}} \;\; \Delta \mathbf{b}^{\mathrm{con}} \,]^T \\ &\qquad - \int_{\Gamma_*^c} [\![\boldsymbol{\Phi}^{\mathrm{con}}]\!]^T \, \boldsymbol{t}^c \, [\, \mathbf{B}_*^{\mathrm{con}} \,] \, \mathrm{d}\Gamma_* \, \Delta \mathbf{q}^{\mathrm{con}} \end{aligned} \tag{40}$$

The term $\Delta \boldsymbol{t}^c$ is the increment of the traction on the crack surface as suggested by Wells et al. [36], $\mathbf{R}$ is the rotation matrix, $\mathbf{T}^c$ is the modulus matrix of the cohesive traction $\boldsymbol{t}_c$ with respect to the crack opening displacement, and

$$\mathbf{B}_*^{\mathrm{con}} = (B_*)_{ikjI} = \frac{1}{2} \, \frac{\partial}{\partial x_k} \, \phi_I^{\mathrm{con}} \left[2 \;\; (H_I^+ + H_I^-) \;\; (\psi_I^+ + \psi_I^-) \right] \delta_{ji} \tag{41}$$

Here H^+, H^- and ψ^+, ψ^- are the values of the enrichment function on the plus and minus sides of the discontinuity Γ_0^c. Because of the shifting operation of Eqs. (19) and (21), $(H_I^+ + H_I^-)$ and $(\psi_I^+ + \psi_I^-)$ do not vanish although sign and sin functions are antisymmetric.

Eq. (35) can be written in a matrix form as

$$[\,\mathbf{K}_{\text{mat}} + \mathbf{K}_{\text{geo}}\,]^k\ \Delta\mathbf{q}^{k+1} = \left\{ \begin{array}{c} \mathbf{r}_f \\ \mathbf{r}_g \end{array} \right\}^k \tag{42}$$

in which $\mathbf{K}_{\text{mat}}$ is the material stiffness matrix and $\mathbf{K}_{\text{geo}}$ is the geometric stiffness. From Eqs. (36) to (40), the material stiffness matrix $\mathbf{K}_{\text{mat}}$ is given by

$$\mathbf{K}_{\text{mat}} = \begin{bmatrix} \mathbf{K}_{\text{uu}}^{\text{ref,ref}} & \mathbf{K}_{\text{uu}}^{\text{ref,con}} & \mathbf{K}_{\text{ua}}^{\text{ref,con}} & \mathbf{K}_{\text{ub}}^{\text{ref,con}} & \mathbf{K}_{\text{u}\Lambda}^{\text{ref},\lambda} \\ \mathbf{K}_{\text{uu}}^{\text{con,ref}} & \mathbf{K}_{\text{uu}}^{\text{con,con}} & \mathbf{K}_{\text{ua}}^{\text{con,con}} & \mathbf{K}_{\text{ub}}^{\text{con,con}} & \mathbf{K}_{\text{u}\Lambda}^{\text{con},\lambda} \\ \mathbf{K}_{\text{au}}^{\text{con,ref}} & \mathbf{K}_{\text{au}}^{\text{con,con}} & \mathbf{K}_{\text{aa}}^{\text{con,con}} & \mathbf{K}_{\text{ab}}^{\text{con,con}} & \mathbf{K}_{\text{a}\Lambda}^{\text{con},\lambda} \\ \mathbf{K}_{\text{bu}}^{\text{con,ref}} & \mathbf{K}_{\text{bu}}^{\text{con,con}} & \mathbf{K}_{\text{ba}}^{\text{con,con}} & \mathbf{K}_{\text{bb}}^{\text{con,con}} & \mathbf{K}_{\text{b}\Lambda}^{\text{con},\lambda} \\ \mathbf{K}_{\Lambda\text{u}}^{\lambda,\text{ref}} & \mathbf{K}_{\Lambda\text{u}}^{\lambda,\text{con}} & \mathbf{K}_{\Lambda\text{a}}^{\lambda,\text{con}} & \mathbf{K}_{\Lambda\text{b}}^{\lambda,\text{con}} & \mathbf{0} \end{bmatrix} \tag{43}$$

where the stiffness matrix $\mathbf{K}_{\text{mat}}$ is symmetric and the terms in the matrix are

$$\begin{aligned}
&\mathbf{K}_{\text{uu}}^{\text{ref,ref}} = \textstyle\int_{\Omega_0^{\text{ref}}} \left[\, \mathbf{B}_{0u}^{\text{ref}} \,\right]^T \mathbf{C}^{\text{ref},S} \left[\, \mathbf{B}_{0u}^{\text{ref}} \,\right] \mathrm{d}\Omega_0 \\
&\mathbf{K}_{\text{u}\Lambda}^{\text{ref},\lambda} = -\textstyle\int_{\Gamma_0^\lambda} \left[\, \boldsymbol{\Phi}_u^{\text{ref}} \,\right]^T \left[\, \boldsymbol{\Phi}_u^{\lambda} \,\right] \mathrm{d}\Gamma_0 \\
&\mathbf{K}_{\text{uu}}^{\text{con,con}} = \textstyle\int_{\Omega_0^{\text{con}}\setminus\Gamma_0^{\text{c}}} [\, \mathbf{B}_{0u}^{\text{con}} \,]^T \mathbf{C}^{\text{con},S} [\, \mathbf{B}_{0u}^{\text{con}} \,] \mathrm{d}\Omega_0 \\
&\mathbf{K}_{\text{ua}}^{\text{con,con}} = \textstyle\int_{\Omega_0^{\text{con}}\setminus\Gamma_0^{\text{c}}} [\, \mathbf{B}_{0u}^{\text{con}} \,]^T \mathbf{C}^{\text{con},S} [\, \mathbf{B}_{0a}^{\text{con}} \,] \mathrm{d}\Omega_0 \\
&\mathbf{K}_{\text{ub}}^{\text{con,con}} = \textstyle\int_{\Omega_0^{\text{con}}\setminus\Gamma_0^{\text{c}}} [\, \mathbf{B}_{0u}^{\text{con}} \,]^T \mathbf{C}^{\text{con},S} [\, \mathbf{B}_{0b}^{\text{con}} \,] \mathrm{d}\Omega_0 \\
&\mathbf{K}_{\text{u}\Lambda}^{\text{con},\lambda} = \textstyle\int_{\Gamma_0^\lambda} [\, \boldsymbol{\Phi}_u^{\text{con}} \,]^T \left[\, \boldsymbol{\Phi}_u^{\lambda} \,\right] \mathrm{d}\Gamma_0 \\
&\mathbf{K}_{\text{aa}}^{\text{con,con}} = \textstyle\int_{\Omega_0^{\text{con}}\setminus\Gamma_0^{\text{c}}} [\, \mathbf{B}_{0a}^{\text{con}} \,]^T \mathbf{C}^{\text{con},S} [\, \mathbf{B}_{0a}^{\text{con}} \,] \mathrm{d}\Omega_0 + \textstyle\int_{\Gamma_*^{\text{c}}} \left[\!\left[\, \boldsymbol{\Phi}_a^{\text{con}} \,\right]\!\right]^T \mathbf{R}\, \mathbf{T}^c\, \mathbf{R}^T \left[\!\left[\, \boldsymbol{\Phi}_a^{\text{con}} \,\right]\!\right] \mathrm{d}\Gamma_* \\
&\mathbf{K}_{\text{ab}}^{\text{con,con}} = \textstyle\int_{\Omega_0^{\text{con}}\setminus\Gamma_0^{\text{c}}} [\, \mathbf{B}_{0a}^{\text{con}} \,]^T \mathbf{C}^{\text{con},S} [\, \mathbf{B}_{0b}^{\text{con}} \,] \mathrm{d}\Omega_0 + \textstyle\int_{\Gamma_*^{\text{c}}} \left[\!\left[\, \boldsymbol{\Phi}_a^{\text{con}} \,\right]\!\right]^T \mathbf{R}\, \mathbf{T}^c\, \mathbf{R}^T \left[\!\left[\, \boldsymbol{\Phi}_b^{\text{con}} \,\right]\!\right] \mathrm{d}\Gamma_* \\
&\mathbf{K}_{\text{a}\Lambda}^{\text{con},\lambda} = \textstyle\int_{\Gamma_0^\lambda} [\, \boldsymbol{\Phi}_a^{\text{con}} \,]^T \left[\, \boldsymbol{\Phi}_u^{\lambda} \,\right] \mathrm{d}\Gamma_0 \\
&\mathbf{K}_{\text{bb}}^{\text{con,con}} = \textstyle\int_{\Omega_0^{\text{con}}\setminus\Gamma_0^{\text{c}}} [\, \mathbf{B}_{0b}^{\text{con}} \,]^T \mathbf{C}^{\text{con},S} [\, \mathbf{B}_{0b}^{\text{con}} \,] \mathrm{d}\Omega_0 + \textstyle\int_{\Gamma_*^{\text{c}}} \left[\!\left[\, \boldsymbol{\Phi}_b^{\text{con}} \,\right]\!\right]^T \mathbf{R}\, \mathbf{T}^c\, \mathbf{R}^T \left[\!\left[\, \boldsymbol{\Phi}_b^{\text{con}} \,\right]\!\right] \mathrm{d}\Gamma_* \\
&\mathbf{K}_{\text{b}\Lambda}^{\text{con},\lambda} = \textstyle\int_{\Gamma_0^\lambda} [\, \boldsymbol{\Phi}_b^{\text{con}} \,]^T \left[\, \boldsymbol{\Phi}_u^{\lambda} \,\right] \mathrm{d}\Gamma_0 \\
&\mathbf{K}_{\text{uu}}^{\text{ref,con}} = \mathbf{K}_{\text{ua}}^{\text{ref,con}} = \mathbf{K}_{\text{ub}}^{\text{ref,con}} = \mathbf{0}
\end{aligned} \tag{44}$$

The same notations as the material stiffness $\mathbf{K}_{\text{mat}}$ are used to represent the terms in the geometric stiffness $\mathbf{K}_{\text{geo}}$ to avoid having too heavy notations. The geometric stiffness $\mathbf{K}_{\text{geo}}$ is not symmetric because of the second term of Eq. (40). The terms of the matrix $\mathbf{K}_{\text{geo}}$ are given by

$$
\begin{aligned}
&\mathbf{K}_{\mathrm{uu}}^{\mathrm{ref,ref}} = \mathbf{I} \int_{\Omega_0^{\mathrm{ref}}} \left[\boldsymbol{\mathcal{B}}_{0u}^{\mathrm{ref}} \right]^T \left\{ \boldsymbol{S}^{\mathrm{ref}} \right\} \left[\boldsymbol{\mathcal{B}}_{0u}^{\mathrm{ref}} \right] \mathrm{d}\Omega_0 \\
&\mathbf{K}_{\mathrm{uu}}^{\mathrm{con,con}} = \mathbf{I} \int_{\Omega_0^{\mathrm{con}} \setminus \Gamma_0^c} [\, \boldsymbol{\mathcal{B}}_{0u}^{\mathrm{con}} \,]^T \{ \boldsymbol{S}^{\mathrm{con}} \} [\, \boldsymbol{\mathcal{B}}^{\mathrm{con}} \,] \, \mathrm{d}\Omega_0 \\
&\mathbf{K}_{\mathrm{ua}}^{\mathrm{con,con}} = \mathbf{K}_{\mathrm{au}}^{\mathrm{con,con}T} = \mathbf{I} \int_{\Omega_0^{\mathrm{con}} \setminus \Gamma_0^c} [\, \boldsymbol{\mathcal{B}}_{0u}^{\mathrm{con}} \,]^T \{ \boldsymbol{S}^{\mathrm{con}} \} [\, \boldsymbol{\mathcal{B}}_{0a}^{\mathrm{con}} \,] \, \mathrm{d}\Omega_0 \\
&\mathbf{K}_{\mathrm{ub}}^{\mathrm{con,con}} = \mathbf{K}_{\mathrm{bu}}^{\mathrm{con,con}T} = \mathbf{I} \int_{\Omega_0^{\mathrm{con}} \setminus \Gamma_0^c} [\, \boldsymbol{\mathcal{B}}_{0u}^{\mathrm{con}} \,]^T \{ \boldsymbol{S}^{\mathrm{con}} \} [\, \boldsymbol{\mathcal{B}}_{0b}^{\mathrm{con}} \,] \, \mathrm{d}\Omega_0 \\
&\mathbf{K}_{\mathrm{aa}}^{\mathrm{con,con}} = \mathbf{I} \int_{\Omega_0^{\mathrm{con}} \setminus \Gamma_0^c} [\, \boldsymbol{\mathcal{B}}_{0a}^{\mathrm{con}} \,]^T \{ \boldsymbol{S}^{\mathrm{con}} \} [\, \boldsymbol{\mathcal{B}}_{0a}^{\mathrm{con}} \,] \, \mathrm{d}\Omega_0 + \int_{\Gamma_*^c} \left[\!\!\left[\boldsymbol{\Phi}_a^{\mathrm{con}} \right]\!\!\right]^T \boldsymbol{t}^c \left[\mathbf{B}_{*,a}^{\mathrm{con}} \right] \mathrm{d}\Gamma_* \\
&\mathbf{K}_{\mathrm{ab}}^{\mathrm{con,con}} = \mathbf{I} \int_{\Omega_0^{\mathrm{con}} \setminus \Gamma_0^c} [\, \boldsymbol{\mathcal{B}}_{0a}^{\mathrm{con}} \,]^T \{ \boldsymbol{S}^{\mathrm{con}} \} [\, \boldsymbol{\mathcal{B}}_{0b}^{\mathrm{con}} \,] \, \mathrm{d}\Omega_0 + \int_{\Gamma_*^c} \left[\!\!\left[\boldsymbol{\Phi}_a^{\mathrm{con}} \right]\!\!\right]^T \boldsymbol{t}^c \left[\mathbf{B}_{*,b}^{\mathrm{con}} \right] \mathrm{d}\Gamma_* \\
&\mathbf{K}_{\mathrm{ba}}^{\mathrm{con,con}} = \mathbf{I} \int_{\Omega_0^{\mathrm{con}} \setminus \Gamma_0^c} [\, \boldsymbol{\mathcal{B}}_{0b}^{\mathrm{con}} \,]^T \{ \boldsymbol{S}^{\mathrm{con}} \} [\, \boldsymbol{\mathcal{B}}_{0a}^{\mathrm{con}} \,] \, \mathrm{d}\Omega_0 + \int_{\Gamma_*^c} \left[\!\!\left[\boldsymbol{\Phi}_b^{\mathrm{con}} \right]\!\!\right]^T \boldsymbol{t}^c \left[\mathbf{B}_{*,a}^{\mathrm{con}} \right] \mathrm{d}\Gamma_* \\
&\mathbf{K}_{\mathrm{bb}}^{\mathrm{con,con}} = \mathbf{I} \int_{\Omega_0^{\mathrm{con}} \setminus \Gamma_0^c} [\, \boldsymbol{\mathcal{B}}_{0b}^{\mathrm{con}} \,]^T \{ \boldsymbol{S}^{\mathrm{con}} \} [\, \boldsymbol{\mathcal{B}}_{0b}^{\mathrm{con}} \,] \, \mathrm{d}\Omega_0 + \int_{\Gamma_*^c} \left[\!\!\left[\boldsymbol{\Phi}_b^{\mathrm{con}} \right]\!\!\right]^T \boldsymbol{t}^c \left[\mathbf{B}_{*,b}^{\mathrm{con}} \right] \mathrm{d}\Gamma_* \\
&\mathbf{K}_{\mathrm{uu}}^{\mathrm{ref,con}} = \mathbf{K}_{\mathrm{ua}}^{\mathrm{ref,con}} = \mathbf{K}_{\mathrm{ub}}^{\mathrm{ref,con}} = \mathbf{K}_{\mathrm{uu}}^{\mathrm{con,ref}} = \mathbf{K}_{\mathrm{au}}^{\mathrm{con,ref}} = \mathbf{K}_{\mathrm{bu}}^{\mathrm{con,ref}} = \mathbf{0} \\
&\mathbf{K}_{\mathrm{u}\Lambda}^{\mathrm{ref},\lambda} = \mathbf{K}_{\mathrm{u}\Lambda}^{\mathrm{con},\lambda} = \mathbf{K}_{\mathrm{a}\Lambda}^{\mathrm{con},\lambda} = \mathbf{K}_{\mathrm{b}\Lambda}^{\mathrm{con},\lambda} = \mathbf{K}_{\Lambda\mathrm{u}}^{\lambda,\mathrm{ref}} = \mathbf{K}_{\Lambda\mathrm{u}}^{\lambda,\mathrm{con}} = \mathbf{K}_{\Lambda\mathrm{a}}^{\lambda,\mathrm{con}} = \mathbf{K}_{\Lambda\mathrm{b}}^{\lambda,\mathrm{con}} = \mathbf{0}
\end{aligned}
\tag{45}
$$

4.2 Deformable interface coupling

In this section, we modify the approach of the last section to allow relative displacements along Γ_0^d and call this *deformable interface coupling*. Therefore, compatibility between the displacement along Γ_0^d is no longer required. Instead, traction boundary conditions are applied depending on the relative displacement $\boldsymbol{g}$ between the reinforcement and the concrete given in Eq. (25):

$$
\begin{aligned}
\boldsymbol{t}_0^{\mathrm{con},d} &= \boldsymbol{t}_0^d(\boldsymbol{g}) \quad \text{on } \Gamma_0 \\
\boldsymbol{t}_0^{\mathrm{ref},d} &= -\boldsymbol{t}_0^d(\boldsymbol{g}) \text{ on } \Gamma_0
\end{aligned}
\tag{46}
$$

The spring modulus depends on the relative displacement and some internal variables. Using (5), we have:

$$
\delta W = \delta W_{\mathrm{ext}} + \delta W_{\mathrm{coh}} + \delta W_{\mathrm{d}} + \delta W_{\mathrm{LM}} - \delta W_{\mathrm{int}} \tag{47}
$$

where δW_{d} is the virtual work by the forces across the interface Γ_0^d. δW_{d} is given by

$$\begin{aligned}\delta W_{\mathrm{d}} &= -\int_{\Gamma_0^d} \delta \boldsymbol{g} \cdot \boldsymbol{t}_0^d \, \mathrm{d}\Gamma_0 \\ &= -\int_{\Gamma_*^d} \delta \boldsymbol{g} \cdot \boldsymbol{t}^d \, \mathrm{d}\Gamma_* \end{aligned} \tag{48}$$

Note that because the traction at the interface depends on the relative displacement, $\boldsymbol{F}_*$ in Eq. (39) is used to map the interface. If no relative displacement is allowed before a certain failure criterion is satisfied, then δW_{LM} should be used.

According to the fundamental lemma of the variational principle, we can obtain the discrete equilibrium equation as before, i.e.

$$\mathbf{r} = \begin{Bmatrix} \mathbf{r}_{\mathrm{f}} \\ \mathbf{r}_{\mathrm{g}} \end{Bmatrix} = \begin{Bmatrix} \mathbf{f}_{\mathrm{ext}} + \mathbf{f}_{\mathrm{coh}} + \mathbf{f}_{\mathrm{d}} + \mathbf{f}_{\mathrm{LM}} - \mathbf{f}_{\mathrm{int}} \\ \mathbf{g} \end{Bmatrix} = \mathbf{0} \tag{49}$$

All other terms are identical to those in Eqs. (28) to (32) but the force for the interface is given by

$$\mathbf{f}_{\mathrm{d}} = -\int_{\Gamma_0^d} \left[\, \boldsymbol{\Phi}^{\mathrm{d}} \, \right]^T \boldsymbol{t}_0^d \, \mathrm{d}\Gamma_0 \tag{50}$$

where $\boldsymbol{\Phi}^{\mathrm{d}} = \begin{bmatrix} \boldsymbol{\Phi}_u^{\mathrm{ref}} & -\boldsymbol{\Phi}_u^{\mathrm{con}} & -\boldsymbol{\Phi}_a^{\mathrm{con}} & -\boldsymbol{\Phi}_b^{\mathrm{con}} \end{bmatrix}$. It is convenient to derive the increment of $\mathbf{f}_{\mathrm{d}}$ in the current configuration that is similar to $\mathbf{f}_{\mathrm{coh}}$.

$$\Delta \boldsymbol{f}_{\mathrm{d}} = -\int_{\Gamma_*^d} \left[\boldsymbol{\Phi}^{\mathrm{d}} \right]^T \mathbf{R} \, \mathbf{T}^d \, \mathbf{R}^T \left[\boldsymbol{\Phi}^{\mathrm{d}} \right] \mathrm{d}\Gamma_* \, \Delta \mathbf{q}^{\mathrm{d}} - \int_{\Gamma_*^d} \left[\boldsymbol{\Phi}^{\mathrm{d}} \right]^T \boldsymbol{t}^d \left[\, \mathbf{B}_*^{\mathrm{d}} \, \right] \mathrm{d}\Gamma_* \, \Delta \mathbf{q}^{\mathrm{d}} \tag{51}$$

in which $\mathbf{T}^d$ is the modulus matrix of the interface traction $\boldsymbol{t}^d$ and $\mathbf{q}^{\mathrm{d}} = [\, \mathbf{u}^{\mathrm{ref}} \;\; \mathbf{u}^{\mathrm{con}} \;\; \mathbf{a}^{\mathrm{con}} \;\; \mathbf{b}^{\mathrm{con}} \,]^T$.

Because the interface is deformable, several terms of the stiffness matrices $\mathbf{K}_{\mathrm{mat}}$ and $\mathbf{K}_{\mathrm{geo}}$ should be modified. The terms to be modified for $\mathbf{K}_{\mathrm{mat}}$ are given by

$$
\begin{aligned}
\mathbf{K}_{\mathrm{uu}}^{\mathrm{ref,ref}} &= \textstyle\int_{\Omega_0^{\mathrm{ref}}} \left[\, \mathbf{B}_{0u}^{\mathrm{ref}} \right]^T \mathbf{C}^{\mathrm{ref},S} \left[\, \mathbf{B}_{0u}^{\mathrm{ref}} \right] \mathrm{d}\Omega_0 + \int_{\Gamma_*^d} \left[\boldsymbol{\Phi}_u^{\mathrm{ref}} \right]^T \mathbf{R}\,\mathbf{T}^d\,\mathbf{R}^T \left[\boldsymbol{\Phi}_u^{\mathrm{ref}} \right] \mathrm{d}\Gamma_* \\
\mathbf{K}_{\mathrm{uu}}^{\mathrm{ref,con}} &= -\textstyle\int_{\Gamma_*^d} \left[\boldsymbol{\Phi}_u^{\mathrm{ref}} \right]^T \mathbf{R}\,\mathbf{T}^d\,\mathbf{R}^T \left[\boldsymbol{\Phi}_u^{\mathrm{con}} \right] \mathrm{d}\Gamma_* \\
\mathbf{K}_{\mathrm{ua}}^{\mathrm{ref,con}} &= -\textstyle\int_{\Gamma_*^d} \left[\boldsymbol{\Phi}_u^{\mathrm{ref}} \right]^T \mathbf{R}\,\mathbf{T}^d\,\mathbf{R}^T \left[\boldsymbol{\Phi}_a^{\mathrm{con}} \right] \mathrm{d}\Gamma_* \\
\mathbf{K}_{\mathrm{ub}}^{\mathrm{ref,con}} &= -\textstyle\int_{\Gamma_*^d} \left[\boldsymbol{\Phi}_u^{\mathrm{ref}} \right]^T \mathbf{R}\,\mathbf{T}^d\,\mathbf{R}^T \left[\boldsymbol{\Phi}_b^{\mathrm{con}} \right] \mathrm{d}\Gamma_* \\
\mathbf{K}_{\mathrm{uu}}^{\mathrm{con,con}} &= \textstyle\int_{\Omega_0^{\mathrm{con}} \setminus \Gamma_0^c} \left[\, \mathbf{B}_{0u}^{\mathrm{con}} \right]^T \mathbf{C}^{\mathrm{con},S} \left[\, \mathbf{B}_{0u}^{\mathrm{con}} \right] \mathrm{d}\Omega_0 + \int_{\Gamma_*^d} \left[\boldsymbol{\Phi}_u^{\mathrm{con}} \right]^T \mathbf{R}\,\mathbf{T}^d\,\mathbf{R}^T \left[\boldsymbol{\Phi}_u^{\mathrm{con}} \right] \mathrm{d}\Gamma_* \\
\mathbf{K}_{\mathrm{ua}}^{\mathrm{con,con}} &= \textstyle\int_{\Omega_0^{\mathrm{con}} \setminus \Gamma_0^c} \left[\, \mathbf{B}_{0u}^{\mathrm{con}} \right]^T \mathbf{C}^{\mathrm{con},S} \left[\, \mathbf{B}_{0a}^{\mathrm{con}} \right] \mathrm{d}\Omega_0 + \int_{\Gamma_*^d} \left[\boldsymbol{\Phi}_u^{\mathrm{con}} \right]^T \mathbf{R}\,\mathbf{T}^d\,\mathbf{R}^T \left[\boldsymbol{\Phi}_a^{\mathrm{con}} \right] \mathrm{d}\Gamma_* \\
\mathbf{K}_{\mathrm{ub}}^{\mathrm{con,con}} &= \textstyle\int_{\Omega_0^{\mathrm{con}} \setminus \Gamma_0^c} \left[\, \mathbf{B}_{0u}^{\mathrm{con}} \right]^T \mathbf{C}^{\mathrm{con},S} \left[\, \mathbf{B}_{0b}^{\mathrm{con}} \right] \mathrm{d}\Omega_0 + \int_{\Gamma_*^d} \left[\boldsymbol{\Phi}_u^{\mathrm{con}} \right]^T \mathbf{R}\,\mathbf{T}^d\,\mathbf{R}^T \left[\boldsymbol{\Phi}_b^{\mathrm{con}} \right] \mathrm{d}\Gamma_* \\
\mathbf{K}_{\mathrm{aa}}^{\mathrm{con,con}} &= \textstyle\int_{\Omega_0^{\mathrm{con}} \setminus \Gamma_0^c} \left[\, \mathbf{B}_{0a}^{\mathrm{con}} \right]^T \mathbf{C}^{\mathrm{con},S} \left[\, \mathbf{B}_{0a}^{\mathrm{con}} \right] \mathrm{d}\Omega_0 \\
&\quad + \textstyle\int_{\Gamma_*^c} \left[\!\left[\boldsymbol{\Phi}_a^{\mathrm{con}} \right]\!\right]^T \mathbf{R}\,\mathbf{T}^c\,\mathbf{R}^T \left[\!\left[\boldsymbol{\Phi}_a^{\mathrm{con}} \right]\!\right] \mathrm{d}\Gamma_* + \int_{\Gamma_*^d} \left[\boldsymbol{\Phi}_a^{\mathrm{con}} \right]^T \mathbf{R}\,\mathbf{T}^d\,\mathbf{R}^T \left[\boldsymbol{\Phi}_a^{\mathrm{con}} \right] \mathrm{d}\Gamma_* \\
\mathbf{K}_{\mathrm{ab}}^{\mathrm{con,con}} &= \textstyle\int_{\Omega_0^{\mathrm{con}} \setminus \Gamma_0^c} \left[\, \mathbf{B}_{0a}^{\mathrm{con}} \right]^T \mathbf{C}^{\mathrm{con},S} \left[\, \mathbf{B}_{0b}^{\mathrm{con}} \right] \mathrm{d}\Omega_0 \\
&\quad + \textstyle\int_{\Gamma_*^c} \left[\!\left[\boldsymbol{\Phi}_a^{\mathrm{con}} \right]\!\right]^T \mathbf{R}\,\mathbf{T}^c\,\mathbf{R}^T \left[\!\left[\boldsymbol{\Phi}_b^{\mathrm{con}} \right]\!\right] \mathrm{d}\Gamma_* + \int_{\Gamma_*^d} \left[\boldsymbol{\Phi}_a^{\mathrm{con}} \right]^T \mathbf{R}\,\mathbf{T}^d\,\mathbf{R}^T \left[\boldsymbol{\Phi}_b^{\mathrm{con}} \right] \mathrm{d}\Gamma_* \\
\mathbf{K}_{\mathrm{bb}}^{\mathrm{con,con}} &= \textstyle\int_{\Omega_0^{\mathrm{con}} \setminus \Gamma_0^c} \left[\, \mathbf{B}_{0b}^{\mathrm{con}} \right]^T \mathbf{C}^{\mathrm{con},S} \left[\, \mathbf{B}_{0b}^{\mathrm{con}} \right] \mathrm{d}\Omega_0 \\
&\quad + \textstyle\int_{\Gamma_*^c} \left[\!\left[\boldsymbol{\Phi}_b^{\mathrm{con}} \right]\!\right]^T \mathbf{R}\,\mathbf{T}^c\,\mathbf{R}^T \left[\!\left[\boldsymbol{\Phi}_b^{\mathrm{con}} \right]\!\right] \mathrm{d}\Gamma_* + \int_{\Gamma_*^d} \left[\boldsymbol{\Phi}_b^{\mathrm{con}} \right]^T \mathbf{R}\,\mathbf{T}^d\,\mathbf{R}^T \left[\boldsymbol{\Phi}_b^{\mathrm{con}} \right] \mathrm{d}\Gamma_*
\end{aligned}
\tag{52}
$$

The terms to modified for $\mathbf{K}_{\text{geo}}$ are given by,

$$
\begin{aligned}
\mathbf{K}_{\text{uu}}^{\text{ref,ref}} &= \mathbf{I} \int_{\Omega_0^{\text{ref}}} \left[\boldsymbol{\mathcal{B}}_{0u}^{\text{ref}} \right]^T \left\{ \boldsymbol{S}^{\text{ref}} \right\} \left[\boldsymbol{\mathcal{B}}_{0u}^{\text{ref}} \right] \, \mathrm{d}\Omega_0 + \int_{\Gamma_*^d} \left[\boldsymbol{\Phi}_u^{\text{ref}} \right]^T \boldsymbol{t}^d \left[\mathbf{B}_{*,u}^{\text{ref}} \right] \, \mathrm{d}\Gamma_* \\
\mathbf{K}_{\text{uu}}^{\text{ref,con}} &= - \int_{\Gamma_*^d} \left[\boldsymbol{\Phi}_u^{\text{ref}} \right]^T \boldsymbol{t}^d \left[\mathbf{B}_{*,u}^{\text{con}} \right] \, \mathrm{d}\Gamma_* \\
\mathbf{K}_{\text{ua}}^{\text{ref,con}} &= - \int_{\Gamma_*^d} \left[\boldsymbol{\Phi}_u^{\text{ref}} \right]^T \boldsymbol{t}^d \left[\mathbf{B}_{*,a}^{\text{con}} \right] \, \mathrm{d}\Gamma_* \\
\mathbf{K}_{\text{ub}}^{\text{ref,con}} &= - \int_{\Gamma_*^d} \left[\boldsymbol{\Phi}_u^{\text{ref}} \right]^T \boldsymbol{t}^d \left[\mathbf{B}_{*,b}^{\text{con}} \right] \, \mathrm{d}\Gamma_* \\
\mathbf{K}_{\text{uu}}^{\text{con,ref}} &= - \int_{\Gamma_*^d} \left[\boldsymbol{\Phi}_u^{\text{con}} \right]^T \boldsymbol{t}^d \left[\mathbf{B}_{*,u}^{\text{ref}} \right] \, \mathrm{d}\Gamma_* \\
\mathbf{K}_{\text{uu}}^{\text{con,con}} &= \mathbf{I} \int_{\Omega_0^{\text{con}} \setminus \Gamma_0^c} \left[\boldsymbol{\mathcal{B}}_{0u}^{\text{con}} \right]^T \left\{ \boldsymbol{S}^{\text{con}} \right\} \left[\boldsymbol{\mathcal{B}}^{\text{con}} \right] \, \mathrm{d}\Omega_0 + \int_{\Gamma_*^d} \left[\boldsymbol{\Phi}_u^{\text{con}} \right]^T \boldsymbol{t}^d \left[\mathbf{B}_{*,u}^{\text{con}} \right] \, \mathrm{d}\Gamma_* \\
\mathbf{K}_{\text{ua}}^{\text{con,con}} &= \mathbf{I} \int_{\Omega_0^{\text{con}} \setminus \Gamma_0^c} \left[\boldsymbol{\mathcal{B}}_{0u}^{\text{con}} \right]^T \left\{ \boldsymbol{S}^{\text{con}} \right\} \left[\boldsymbol{\mathcal{B}}_{0a}^{\text{con}} \right] \, \mathrm{d}\Omega_0 + \int_{\Gamma_*^d} \left[\boldsymbol{\Phi}_u^{\text{con}} \right]^T \boldsymbol{t}^d \left[\mathbf{B}_{*,a}^{\text{con}} \right] \, \mathrm{d}\Gamma_* \\
\mathbf{K}_{\text{ub}}^{\text{con,con}} &= \mathbf{I} \int_{\Omega_0^{\text{con}} \setminus \Gamma_0^c} \left[\boldsymbol{\mathcal{B}}_{0u}^{\text{con}} \right]^T \left\{ \boldsymbol{S}^{\text{con}} \right\} \left[\boldsymbol{\mathcal{B}}_{0b}^{\text{con}} \right] \, \mathrm{d}\Omega_0 + \int_{\Gamma_*^d} \left[\boldsymbol{\Phi}_u^{\text{con}} \right]^T \boldsymbol{t}^d \left[\mathbf{B}_{*,b}^{\text{con}} \right] \, \mathrm{d}\Gamma_* \\
\mathbf{K}_{\text{au}}^{\text{con,ref}} &= - \int_{\Gamma_*^d} \left[\boldsymbol{\Phi}_a^{\text{con}} \right]^T \boldsymbol{t}^d \left[\mathbf{B}_{*,u}^{\text{ref}} \right] \, \mathrm{d}\Gamma_* \\
\mathbf{K}_{\text{au}}^{\text{con,con}} &= \int_{\Gamma_*^d} \left[\boldsymbol{\Phi}_a^{\text{con}} \right]^T \boldsymbol{t}^d \left[\mathbf{B}_{*,u}^{\text{con}} \right] \, \mathrm{d}\Gamma_* \\
\mathbf{K}_{\text{aa}}^{\text{con,con}} &= \mathbf{I} \int_{\Omega_0^{\text{con}} \setminus \Gamma_0^c} \left[\boldsymbol{\mathcal{B}}_{0a}^{\text{con}} \right]^T \left\{ \boldsymbol{S}^{\text{con}} \right\} \left[\boldsymbol{\mathcal{B}}_{0a}^{\text{con}} \right] \, \mathrm{d}\Omega_0 \\
&\quad + \int_{\Gamma_*^c} \left[\!\!\left[\boldsymbol{\Phi}_a^{\text{con}} \right]\!\!\right]^T \boldsymbol{t}^c \left[\mathbf{B}_{*,a}^{\text{con}} \right] \, \mathrm{d}\Gamma_* + \int_{\Gamma_*^d} \left[\boldsymbol{\Phi}_u^{\text{con}} \right]^T \boldsymbol{t}^d \left[\mathbf{B}_{*,u}^{\text{con}} \right] \, \mathrm{d}\Gamma_* \\
\mathbf{K}_{\text{ab}}^{\text{con,con}} &= \mathbf{I} \int_{\Omega_0^{\text{con}} \setminus \Gamma_0^c} \left[\boldsymbol{\mathcal{B}}_{0a}^{\text{con}} \right]^T \left\{ \boldsymbol{S}^{\text{con}} \right\} \left[\boldsymbol{\mathcal{B}}_{0b}^{\text{con}} \right] \, \mathrm{d}\Omega_0 \\
&\quad + \int_{\Gamma_*^c} \left[\!\!\left[\boldsymbol{\Phi}_a^{\text{con}} \right]\!\!\right]^T \boldsymbol{t}^c \left[\mathbf{B}_{*,b}^{\text{con}} \right] \, \mathrm{d}\Gamma_* + \int_{\Gamma_*^d} \left[\boldsymbol{\Phi}_a^{\text{con}} \right]^T \boldsymbol{t}^d \left[\mathbf{B}_{*,b}^{\text{con}} \right] \, \mathrm{d}\Gamma_* \\
\mathbf{K}_{\text{bu}}^{\text{con,ref}} &= - \int_{\Gamma_*^d} \left[\boldsymbol{\Phi}_b^{\text{con}} \right]^T \boldsymbol{t}^d \left[\mathbf{B}_{*,u}^{\text{ref}} \right] \, \mathrm{d}\Gamma_* \\
\mathbf{K}_{\text{bu}}^{\text{con,con}} &= \int_{\Gamma_*^d} \left[\boldsymbol{\Phi}_b^{\text{con}} \right]^T \boldsymbol{t}^d \left[\mathbf{B}_{*,u}^{\text{con}} \right] \, \mathrm{d}\Gamma_* \\
\mathbf{K}_{\text{ba}}^{\text{con,con}} &= \mathbf{I} \int_{\Omega_0^{\text{con}} \setminus \Gamma_0^c} \left[\boldsymbol{\mathcal{B}}_{0b}^{\text{con}} \right]^T \left\{ \boldsymbol{S}^{\text{con}} \right\} \left[\boldsymbol{\mathcal{B}}_{0a}^{\text{con}} \right] \, \mathrm{d}\Omega_0 \\
&\quad + \int_{\Gamma_*^c} \left[\!\!\left[\boldsymbol{\Phi}_b^{\text{con}} \right]\!\!\right]^T \boldsymbol{t}^c \left[\mathbf{B}_{*,a}^{\text{con}} \right] \, \mathrm{d}\Gamma_* + \int_{\Gamma_*^d} \left[\boldsymbol{\Phi}_b^{\text{con}} \right]^T \boldsymbol{t}^d \left[\mathbf{B}_{*,a}^{\text{con}} \right] \, \mathrm{d}\Gamma_* \\
\mathbf{K}_{\text{bb}}^{\text{con,con}} &= \mathbf{I} \int_{\Omega_0^{\text{con}} \setminus \Gamma_0^c} \left[\boldsymbol{\mathcal{B}}_{0b}^{\text{con}} \right]^T \left\{ \boldsymbol{S}^{\text{con}} \right\} \left[\boldsymbol{\mathcal{B}}_{0b}^{\text{con}} \right] \, \mathrm{d}\Omega_0 \\
&\quad + \int_{\Gamma_*^c} \left[\!\!\left[\boldsymbol{\Phi}_b^{\text{con}} \right]\!\!\right]^T \boldsymbol{t}^c \left[\mathbf{B}_{*,b}^{\text{con}} \right] \, \mathrm{d}\Gamma_* + \int_{\Gamma_*^d} \left[\boldsymbol{\Phi}_b^{\text{con}} \right]^T \boldsymbol{t}^d \left[\mathbf{B}_{*,b}^{\text{con}} \right] \, \mathrm{d}\Gamma_*
\end{aligned}
\tag{53}
$$

The discrete equations are evaluated by using the standard Gauss quadrature for both the finite element and particle domains. For the particle domain, a background mesh is used where the particles form rectangular background cells. The 4×4 Gauss points were used for numerical integration.

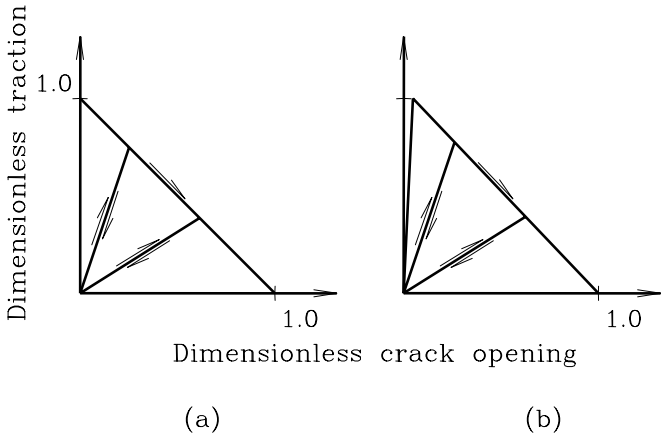

Fig. 3. (a) The rigid cohesive model and (b) the non-rigid cohesive model, where the traction and the crack opening displacement are nondimensionalized by the tensile strength and the critical crack opening displacement.

5 Constitutive models

The steel reinforcement is modeled with an elastoplastic constitutive model with isotropic hardening. Details can be found elsewhere such as [37]. To model the concrete, we used a linear elasticity for the tension and a continuum scalar damage model for the compression [38]. If the principal tensile stress exceeds the tensile of the concrete, a crack is initiated, i.e. we used the Rankine criterion to initiate the crack.

Once the criterion for the crack initiation is satisfied near a particle, the cohesive crack model is introduced at the particle. We used a linear rigid and in some cases a bilinear non-rigid cohesive model as shown in Fig. 3. In each case we specified the fracture energy G_f and the tensile strength f_t as material parameters.

The actual bond behavior depends on the surface of the reinforcement bars. For bars without ribs, adhesion and friction are the principal mechanisms of bonding. For ribbed bars, the bond behavior is the result of a very complicated mechanism in a small region called effective concrete cover c_{eff} (Fig. 4). A bond model developed by Rabczuk and Belytschko was used in this paper. The detailed information of the bond model can be found in [30] and the

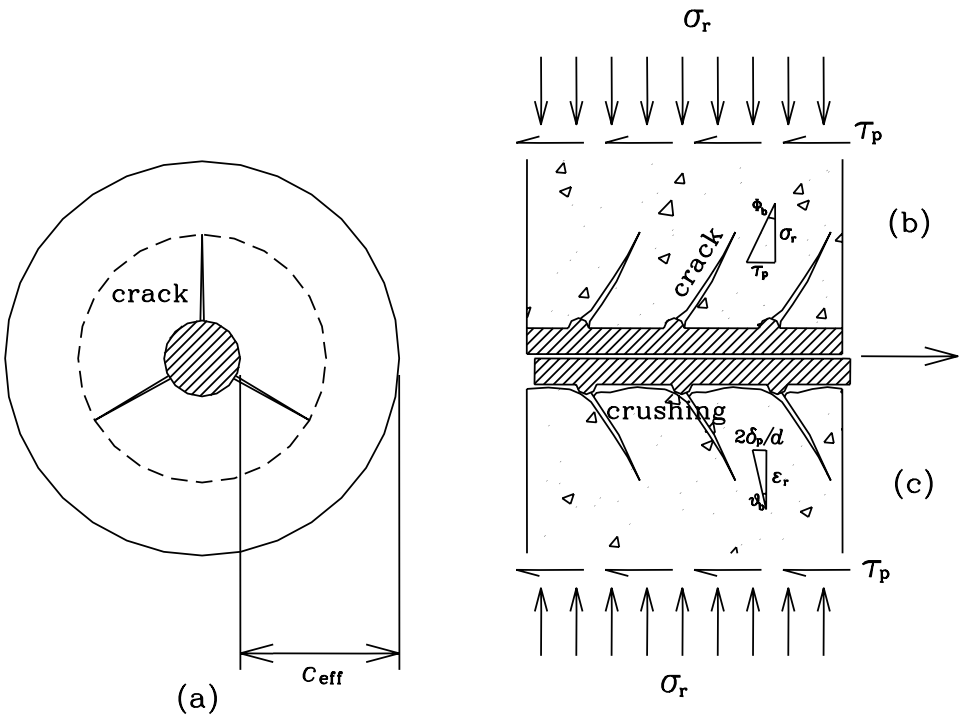

Fig. 4. (a) The development of radial cracks in the effective concrete cover surrounding the reinforcement, (b) the mechanical interaction of the cracked concrete and the rib and (c) the crushed concrete near the reinforcement when the reinforcement is pulled out.

references therein.

6 Application examples

6.1 Prestressed concrete beams

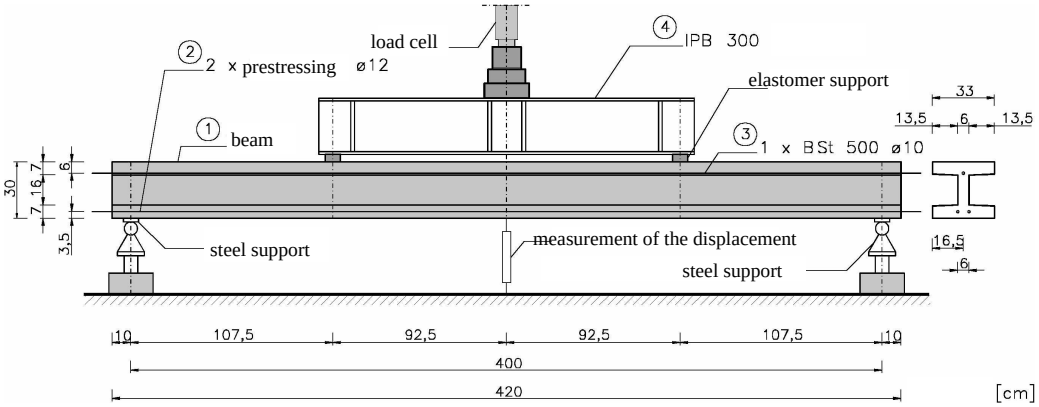

Fig. 5. The test set-up of beam I

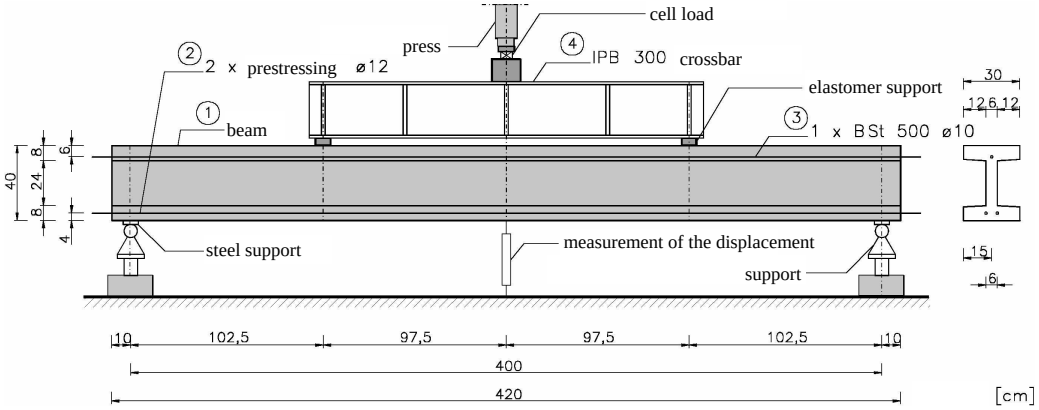

Fig. 6. The test set-up of beam II

We considered two prestressed four-point bending concrete beams without the shear stirrups. Both beams had an I-shaped cross section as illustrated in Figs. 5 and 6. The test setup and the dimensions of the beam are illustrated in Figs. 5 and 6. Two different kinds of reinforcements were used. The beams had two tension wires in the lower flange that were prestressed. The upper reinforcement was only needed for transportation purposes. The lower reinforcement had a diameter of 12 mm and the diameter of the upper reinforcement was 10 mm. The two tension wires of beam I were prestressed each with a force

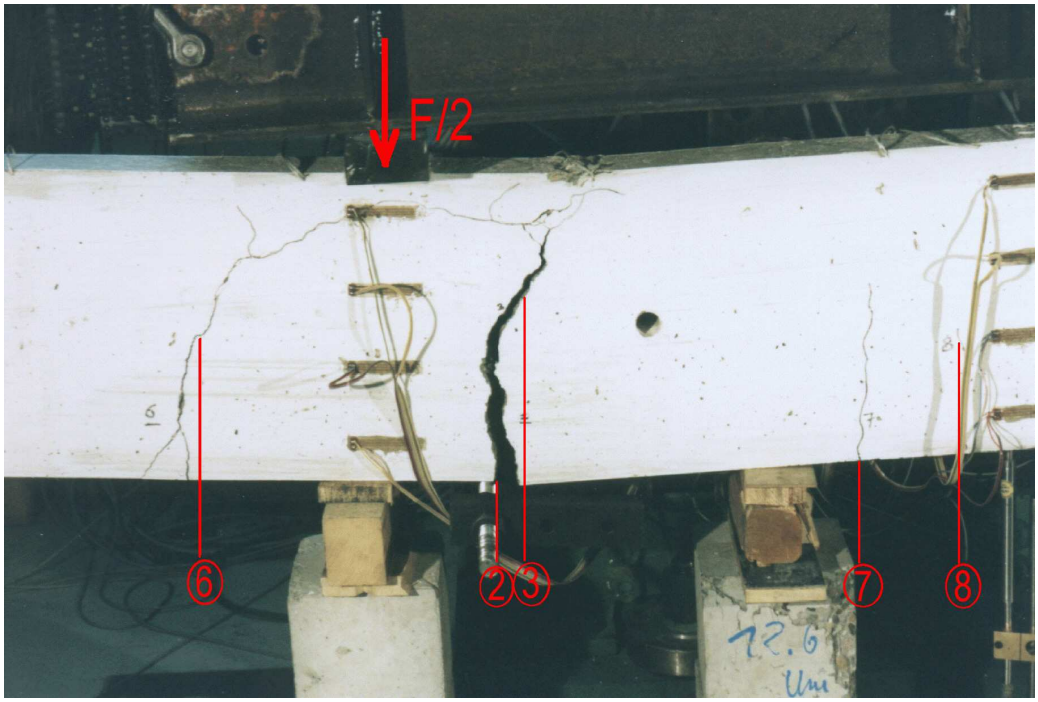

Fig. 7. (a) Beam II after the experiment and (b) beam I after the experiment

of 68 kN, the wires of the second beam with a force of 80 kN. The wires were first prestressed, then concreted and after the concrete had reached 80% of its compressive strength, the prestressing was relieved such that the forces from the reinforcement were transmitted into the concrete. The experiment was done displacement-controlled; see [40]. Both beams failed due to a combined shear/pullout failure as illustrated in Fig. 7.

The concrete tensile strength was $f_t = 2.8$ MPa, Young's modulus $E = 29$ GPa, Poisson's ratio $\nu = 0.2$, compressive strength $f_c = 45$ MPa and fracture energy $G_f = 86$ N/m. The yield strength for the usual reinforcements was from 500 MPa with a Young's modulus 210 GPa. The yield strength for the prestressed tendons was 1,420 MPa with a Young's modulus of 205 GPa. More details about the experiments can be found in [41].

We used the bond model given in Section **??** to model the complicated bond mechanism in the small region surrounding the reinforcement. Otherwise, the correct failure pattern cannot be reproduced since the final failure of the beam is caused by a pullout-failure. Beam elements were used for the reinforcement and meshfree EFG nodes for the concrete. We used an unstructured particle

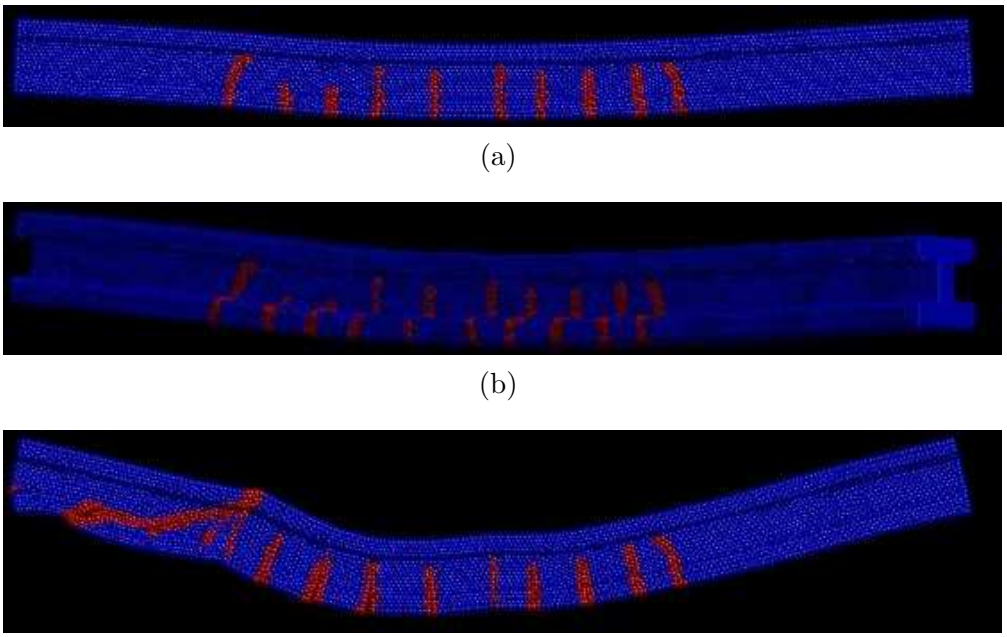

(a)

(b)

(c)

Fig. 8. The crack pattern for beam I at different load steps for the fine computation where the displacement was exaggerated 5 times .

arrangement with different numbers of particles and used adaptivity to keep the computational cost low. The adaptive procedure is explained in [42, 43]. To solve the linearized systems of equations we employed the parallel open source direct solver package SPOOLES. The computations were carried out on a parallel cluster that used up to 16 processors. To avoid an unrealistic symmetric crack pattern, we varied the material strength in the specimen, meaning we multiplied the stress-strain curve with a small factor of $0.98 \leq \alpha \leq 1.02$, obtained from a log-normal distribution around a mean value of 1 and a standard deviation of 2%.

The prestressing was modeled via a virtual temperature change in the tension wires such that the tension wire was shortened by cooling down. The strains were computed by $\epsilon = \alpha_t \ \Delta T$ where α_t was the thermal expansion coefficient which was 1×10^{-5}°C for steel and ΔT was the temperature difference, which was negative in our case. The contraction of the tension wire transmitted the prestressing forces in the concrete.

Figs. 8 and 9 show the deformed concrete beam I in the current configuration at

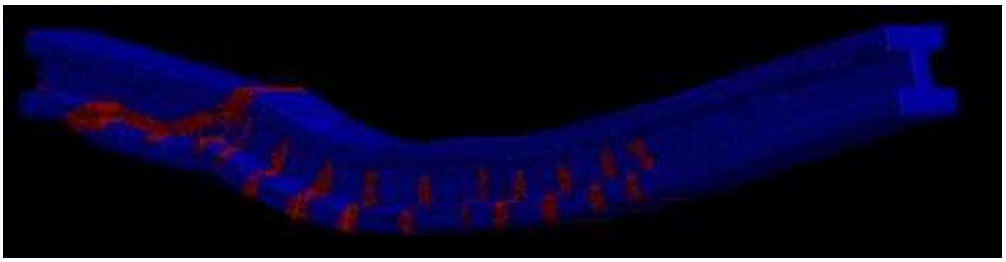

(a)

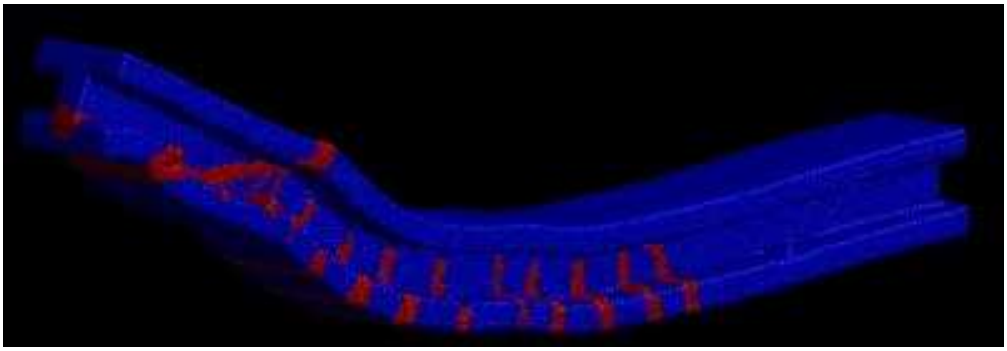

(b)

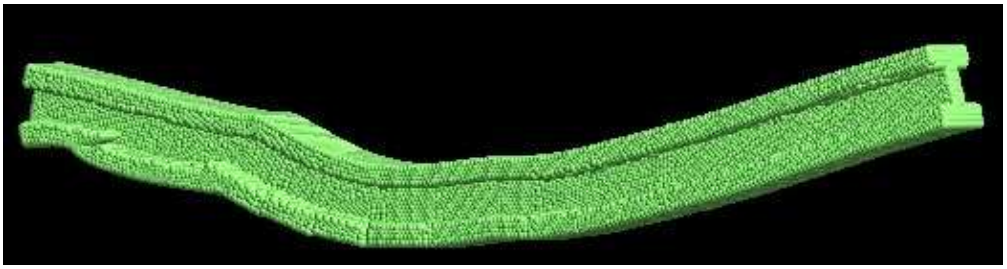

(c)

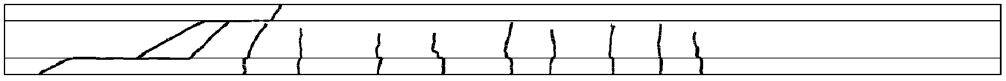

(d)

Fig. 9. The final crack pattern for beam I for the fine computation and for different view points; (a)-(c) numerical simulation, (d) experiment

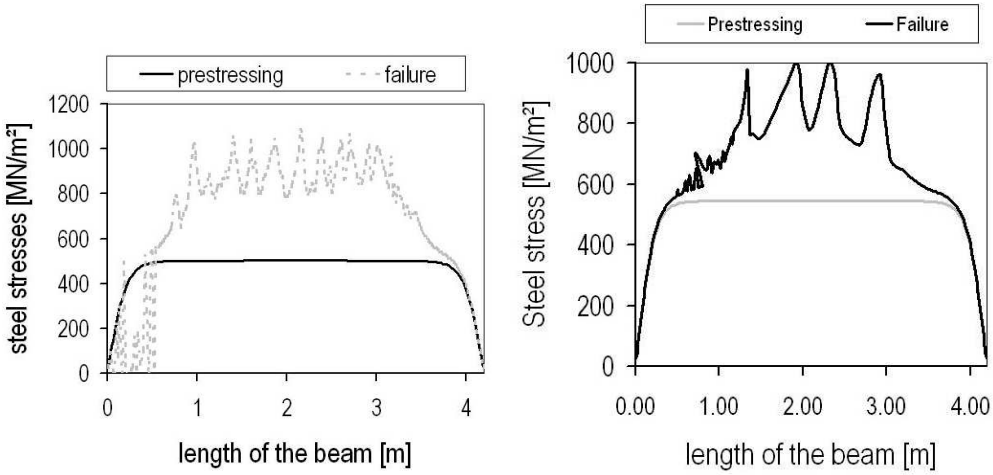

(a) Beam I (b) Beam II

Fig. 10. The tensile stress of a tendon just after prestressing and at failure.

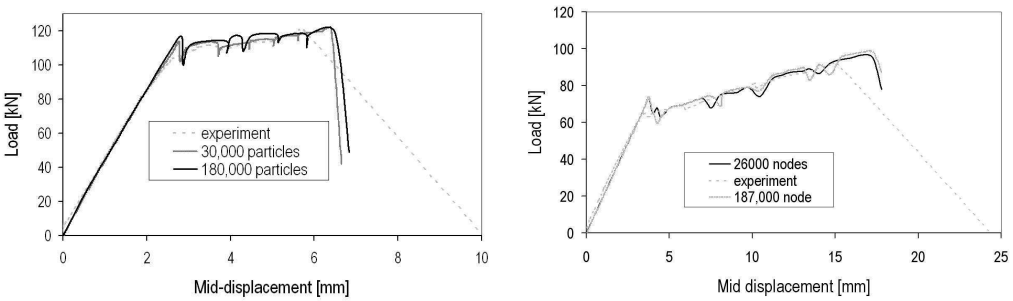

(a) Beam I (b) Beam II

Fig. 11. The load deflection curves for the prestressed concrete beam problem

different load steps and for different points of view. The deformation plots were magnified to better illustrate the crack opening. Moreover, particles adjacent to the crack were plotted in red. The final crack patterns agreed well with the experimental failure pattern shown in Fig. 9d. Fig. 10a shows the steel stresses at prestressing and at failure. At prestressing, the stress distribution was, of course, homogenous. At failure, the stress peaks were observed at locations where the concrete cracks and hence the reinforcement had to carry the entire load; we noted that the steel stresses were significantly below the yield strength of the tendon. When the bar was pulled out, the bond was weakened close to the support as indicated by the steel stresses that started oscillating. They did not drop to zero since the bond was not completely destroyed. This was difficult to model in a numerical analysis. The load deflection curve is shown in Fig. 11a. The numerical simulation was able to reproduce the experimental results very well.

The crack pattern (shown in the initial configuration) for beam II is illustrated in Fig. 12. It agreed well with the experiments. Less cracks occurred compared to the failure of beam I. Also the load-deflection curves agreed well as seen in Fig. 11b. The stresses in the tendon at failure and after the prestressing loading case (after the stresses were transmitted into the concrete taking also into account the shortening of the concrete that caused a stress reduction) are shown in Fig. 10 for both beams. As can be seen, the tensile strength in the steel was never exceeded. The beam clearly failed due to a combined shear/anchorage failure.

6.2 The failure of the frame corners

Experiments on the failure of reinforced concrete frame corners subjected to positive and negative moment loading were performed by Akkermann [44]. The experimental set-up is shown in Fig. 13.

The concrete tensile strength was $f_t = 2.6$ MPa, Young's modulus $E = 24$ GPa, compressive strength $f_c = 30$ MPa and fracture energy $G_f = 100$ N/m.

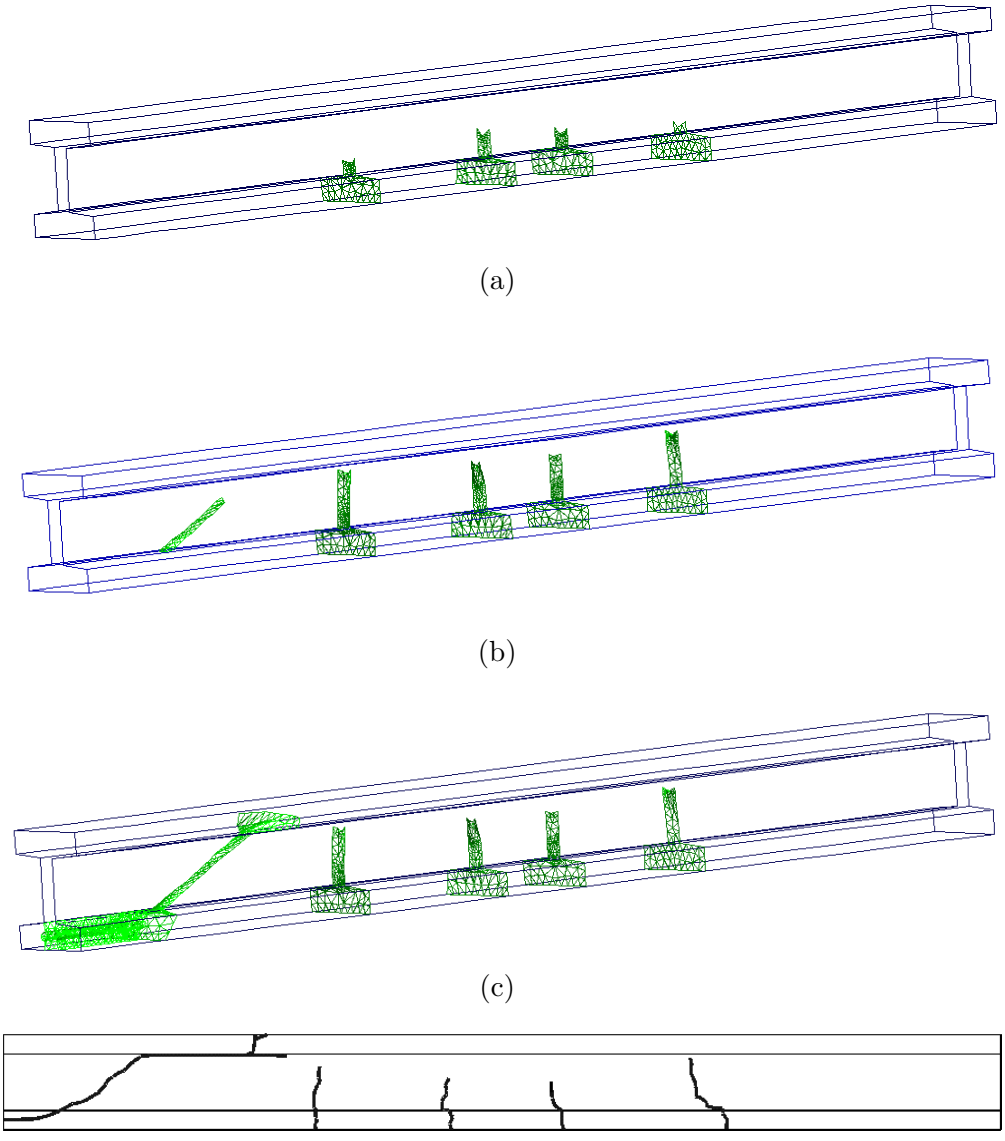

Fig. 12. The crack pattern for beam II at different load steps

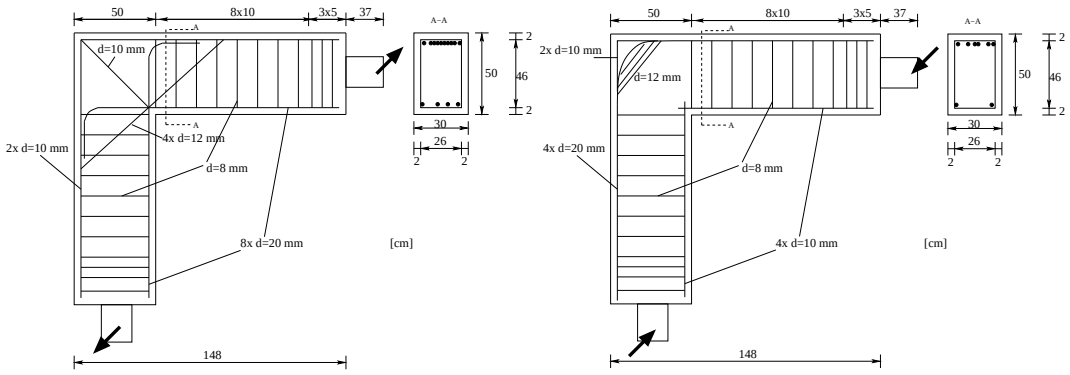

(a) (b)

Fig. 13. The test setup of the frame corners (a) $FC1$ and (b) $FC2$.

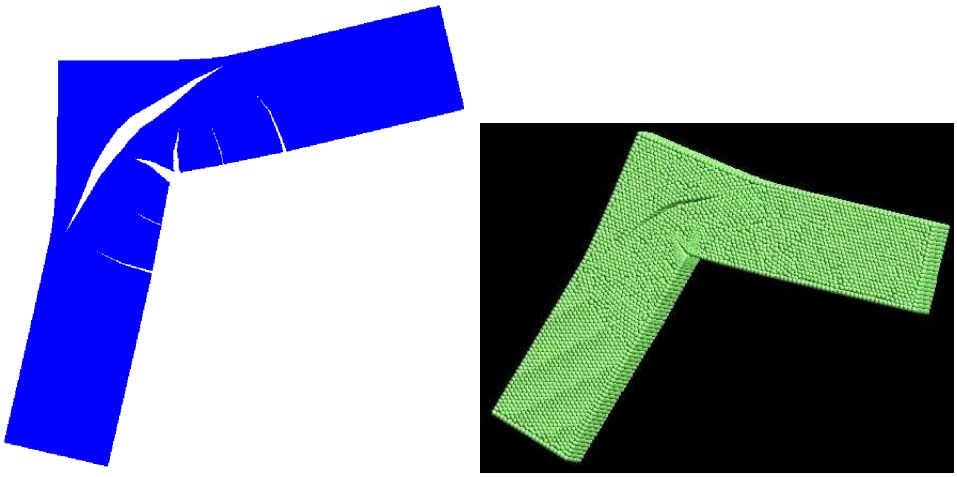

(a) (b)

Fig. 14. Frame corner FC1

Different kind of reinforcements were used as shown in Fig. 13. The yield strength for the different reinforcements ranged from 510 MPa to 603 MPa and the Young's modulus from 180 GPa to 205 GPa. More details about the experiments can be found in [44].

Frame corner FC1 was loaded with a positive moment, see Fig. 13a, and failed due to concrete failure, meaning by the pulling of the corner. The bond behavior was of minor importance in this example. Hence, the reinforcement was connected rigidly to the concrete. We used a structured discretization.

For frame corner FC2, the bond behavior was important. Frame corner FC2 was loaded with a negative moment and failed due to a splitting failure. Since the dimensions of FC1 and FC2 were equivalent, the same structured discretization was used for the concrete.

Fig. 14 shows the final crack pattern of the computation for structure FC1 in a two and three-dimensional view. The diagonal crack caused the failure of the structure. Several small cracks at the inside of the frame corners were observed, which matched well with the experimental data. Fig. 15 shows the crack pattern and the deformed frame corner FC2 at different points of views. The deformations are shown magnified. Fig. 16 shows the stress distribution at the end of the computation in a two-dimensional view for one slab of the

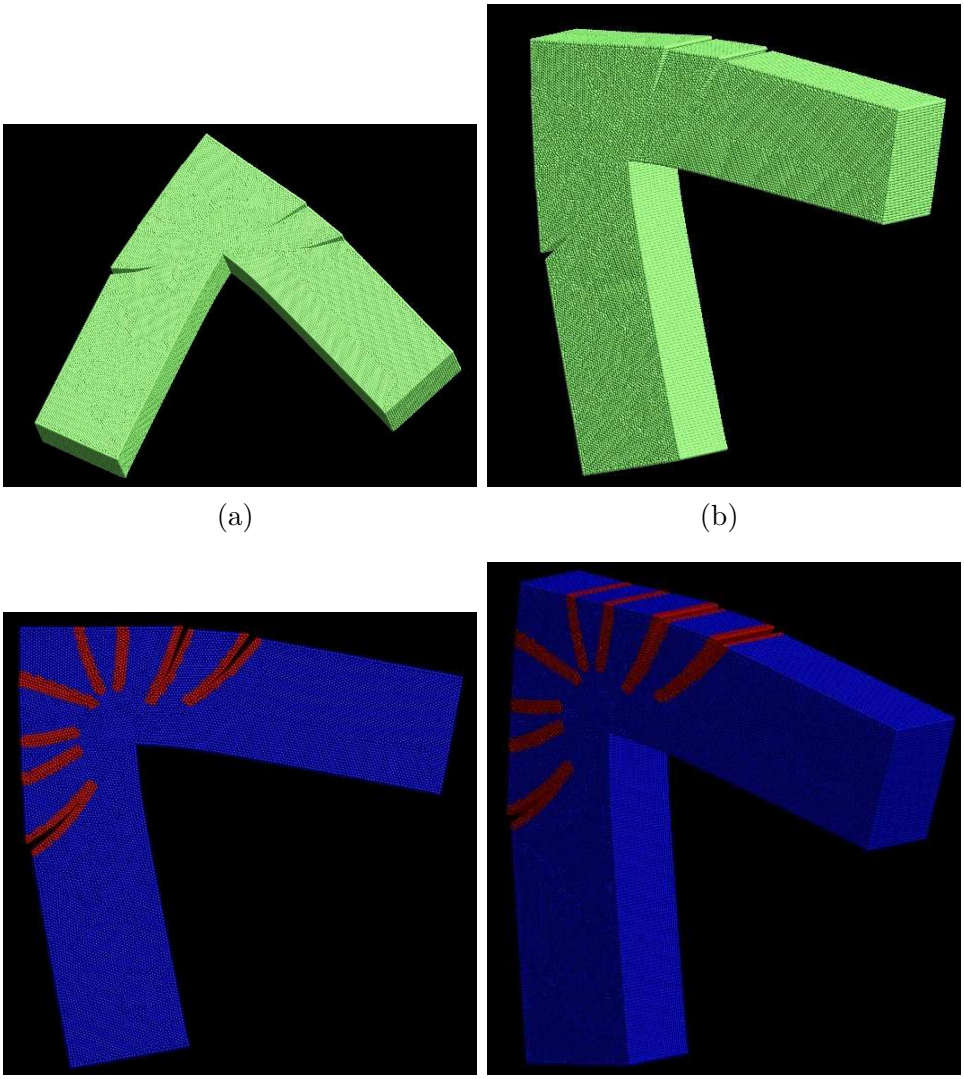

(a) (b)

(c) (d)

Fig. 15. Frame corner FC2, 3D view

(a) (b)

Fig. 16. Frame corner FC2, 2D view

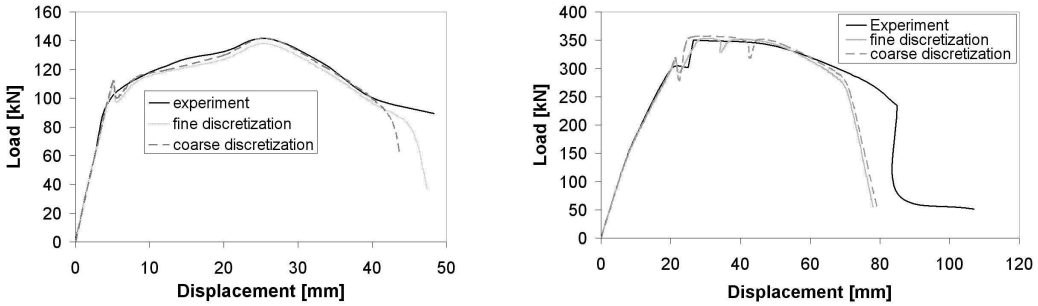

(a) FC1 (b) FC2

Fig. 17. The load displacement curves of frame corners FC1 and FC2 for different numbers of particles

specimen as well as the deformed configuration [3]. The splitting failure was captured by the simulation. Fig. 17 compares the computational and experimental load displacement curves of the two frame corners. They are in good agreement.

7 Summary and discussion

We presented a geometrical and material non-linear three-dimensional reinforced concrete model. A meshfree discretization was used for the concrete. Cracking was realized through the extended element free Galerkin method by explicitly introducing the crack. Nodes whose domain of influence was cut by the crack were enriched with the step function or a near top function. Once a crack was initiated, a cohesive model guaranteed the correct energy dissipation once the crack opens. The prestressing tendons, as well as the "usual" reinforcement were modeled with finite elements using standard J_2-plasticity with isotropic hardening. The reinforcement was coupled to the concrete via a bond model taking into account the pullout- and splitting-failure. In certain cases, i.e. cases where it is obvious that the structure would not fail due to a bond failure, a rigid coupling was used in order to connect the reinforcement to the concrete.

The method was applied to several problems: prestressed concrete beams without stirrup reinforcement and frame corners subjected to a positive and negative moment. In the first case, the beams failed due to a combined shear/anchorage failure. This tendency was captured by a numerical simulation. We note that we were not able to capture this failure mechanism in earlier studies in a 2D-setting [45]. We also were able to capture load-deflection curves.

The frame corners failed either due to a concrete failure or due to a splitting failure. Both failure mechanisms were captured in the numerical simulation. The load deflection curves agreed well with the ones observed in our experi-

[3] illustrated magnified

ments. Rotations played an important role in the frame corner experiments. Therefore, a geometrical nonlinear formulation is essential. Our results improved significantly in comparison to the ones in [30] that used a geometrical linear analysis.

Acknowledgement

The second author would like to thank the Agency for Defense Development (ADD) for grant ADD-06-05-06 and Korea Institute of Construction & Transportation Technology Evaluation and Planning (KICTTEP) for grant 05-CETFC-B01.

References

[1] Lemaitre J. Evaluation of dissipation and damage in metal submitted to dynamic loading, Proc ICM 1 1971.

[2] Hillerborg A, Modéer M, Peterson PE. Analysis of crack formation and crack growth in concrete by means of fracture mechanics and finite elements, Cem and Concr Res 1976;6:773–782.

[3] Bazant Z, Oh B. Crack band theory for fracture in concrete, Mater Struc 1983;16:155–177.

[4] Jirasek M, Zimmermann T. Rotating crack model with transition to scalar damage, ASCE J Engng Mech 1998;124(3):277–284.

[5] Jirasek M, Zimmermann T. Analysis of rotating crack model, ASCE J Engng Mech 1998;124:842–851.

[6] Bažant Z. Why continuum damage is nonlocal: Micromechanics arguments, ASCE J Engng Mech 1991;117(5):1070–1087.

[7] Bažant ZP, Pijaudier-Cabot G. Nonlocal continuum damage, localization instabilities and convergence, ASCE J Engng Mech 1988;55:287–293.

[8] Bažant ZP, Jirasek M. Non-local integral formulations of plasticity and damage: survey of process, ASCE J Engng Mech 2002;128(1):1119–1149.

[9] Bažant ZP. Size effect in blunt fracture: Concrete, rock, metal, ASCE J Engng Mech 1984;110:518–535.

[10] Bažant ZP, Li Z. Modulus of rupture: Size effect due to fracture initiation in boundary layer, ASCE J Engng Mech 1995;121(4):739–746.

[11] Bažant ZP, Yu Q, Zi G., Choice of concrete fracture test for a standard, Int J Fract 2003;118:303–337.

[12] Zi G, Bažant ZP. Eigenvalue method for computing size effect of cohesive cracks with residual stress, with application to kink bands in composites, Int J of Engng Sci 2003;41(13-14):1519–1534.

[13] Peerlings RHJ, de Borst R, Brekelmans WAM, de Vree JHP. Gradient enhanced damage for quasi-brittle materials, Int J Numer Meth Engng 1996;39(19):3391–3403.

[14] Xu XP, Needleman A. Numerical simulations of fast crack growth in brittle solids, J Mech Phys Solids 1994;42:1397–1434.

[15] Xu XP, Needleman A. Void nucleation by inclusion debonding in a crystal matrix, Model Simulat Mater Sci Engng 1993;1:111–132.

[16] Potyondy D, Wawrzynek P, Ingraffea A. An algorithm to generate quadrilaterial or triangular element surface meshes in arbitrayr domains with applications to crack-propagation, Int J Numer Meth Engng 1995;38:2677–2701.

[17] Bittencourt T, Wawrzynek P, Ingraffea A. Quasi-automatic simulation of crack propagation for 2D LEFM problems, Engng Fract Mech 1996;55(2):321–334.

[18] Belytschko T, Black T. Elastic crack growth in finite elements with minimal remeshing, Int J Numer Meth Engng 1999;45(5):601–620.

[19] Belytschko T, Moes N, Usui S, Parimi C. Arbitrary discontinuities in finite elements, Int J Numer Meth Engng 2001;50(4):993–1013.

[20] Moes N, Dolbow J, Belytschko T. A finite element method for crack growth without remeshing, Int J Numer Meth Engng 1999;46(1):133–150.

[21] Zi G, Belytschko T. New crack-tip elements for XFEM and applications to cohesive cracks, Int J Numer Meth Engng 2003;57:2221–2240.

[22] Belytschko T, Lu Y, Gu L. Element-free galerkin methods, Int J Numer

Meth Engng 1994;37:229–256.

[23] Belytschko T, Lu Y, Gu L. Crack propagation by element-free galkerin methods, Engng Fract Mech 1994;51:295–315.

[24] Belytschko T, Lu Y. Element-free galerkin methods for static and dynamic fracture, Int J Solids Struct 1995;32:2547–2570.

[25] Belytschko T, Tabbara M. Dynamic fracture using element-free galerkin methods, Int J Numer Meth Engng 1996;39(6):923–938.

[26] Ventura G, Xu J, Belytschko T. A vector level set method and new discontinuity approximations for crack growth by EFG, Int J Numer Meth Engng 2002;54(6):923–944.

[27] Rabczuk T, Zi G. A meshfree method based on the local partition of unity for cohesive cracks, Comput Mech 2007;39(6):743–760.

[28] Cox J, Herrmann L. Development of a plasticity bond model for steel reinforcement, Mech Coh Fric Mat 1998;3:155–180.

[29] Cox J, Herrmann L. Validation of a plasticity bond model for steel reinforcement, Mech Coh Fric Mat 1999;4:361–389.

[30] Rabczuk T, Belytschko T. Application of meshfree particle methods to static fracture of reinforced concrete structures, Int J Fract 2006;137(1-4):19–49.

[31] Belytschko T, Liu WK, Moran B. Nonlinear Finite Elements for Continua and Structures, John Wiley and Sons, Chichester, 2000.

[32] Belytschko T, Tabbara M. Dynamic fracture using element-free Galerkin methods, Int J Numer Meth Engng 1996;39(6):923–938.

[33] Belytschko T, Lu Y, Gu L. Crack propagation by element-free Galerkin methods, Engng Fract Mech 1995;51(2):295–315.

[34] Zi G, Rabczuk T, Wall W. Extended meshfree methods without the branch enrichment for cohesive cracks, Comput Mech 2007;40(2):367–382.

[35] Bordas S, Rabczuk T, Zi G. Three-dimensional crack initiation, propagation, branching and junction in non-linear materials by an extended meshfree method without asymptotic enrichment, Engng Fract Mech – online, DOI:10.1016/j.engframech.2007.05.010.

[36] Wells GN, de Borst R, Sluys LJ. A consistent geometrically non-linear approach for delamination, Int J Numer Meth Engng 2002;54(9):1333–1355.

[37] Chen W. Constitutive Equations for Engineering Materials, Volume 2: Plasticity and Modeling, Elsevier, Amsterdam-London-New York-Tokio, 1994.

[38] Rabczuk T, Eibl J. Simulation of high velocity concrete fragmentation using sph/mlsph, Int J Numer Meth Engng 2003;56:1421–1444.

[39] Rabczuk T, Bordas S, Zi G. A three-dimensional meshfree method for continuous multiple-crack initiation, propagation and junction in statics and dynamics, Comput Mech 2007;40(3): –in online, DOI:10.1007/s00466–006–0122–1.

[40] Eibl J, Stempniewski L, Rabczuk T. Der endbereich von im werk vorgespannten fertigteiltraegern-hohlplatten, final report, Universitaet Karlsruhe, Institut fuer Massivbau und Baustofftechnologie; 2002.

[41] Stempniewski L, Eibl J, Rabczuk T. Der endbereich von im werk vorgespannten fertigteiltraegern-hohlplatten, Tech. rep., Institut fuer Massivbau und Baustofftechnologie, University of Karlsruhe; 2001.

[42] Rabczuk T, Belytschko T. Adaptivity for structured meshfree particle methods in 2D and 3D, Int J Numer Meth Engng 2005;63(11):1559–1582.

[43] Rabczuk T, Belytschko T. A three dimensional large deformation meshfree method for arbitrary evolving cracks, Comput Meth Appl Mech Engng 2007;196(29-30):2777–2799.

[44] Akkermann J. Rotationsverhalten von stahlbeton-rahmenecken, Ph.D. thesis, University of Karlsruhe, Institute for Concrete Materials; 2000.

[45] Rabczuk T, Akkermann J, Eibl J. A numerical model for reinforced concrete structures, Int J Solids Struct 2005;42(5-6):1327–1354.